spanning the entire SIVmac239 Gag, Pol, Vif, Vpx, Vpr, Tat, Rev, Nef, and Env amino acid sequences. Intracellular IFN-γ staining was performed with a Cytofix-Cytoperm kit (Becton Dickinson, Tokyo, Japan) and fluorescein isothiocyanate-conjugated anti-human CD4 (Becton Dickinson), peridinin chlorophyll protein-conjugated anti-human CD8 (Becton Dickinson), allophycocyanin-conjugated anti-human CD3 (Becton Dickinson), and phycoerythrin-conjugated anti-human IFN-γ monoclonal antibodies (BioLegend, Tokyo, Japan). Specific $CD8^+$ T-cell frequencies were calculated by subtracting nonspecific IFN-γ^+ $CD8^+$ T-cell frequencies from those after peptide-specific stimulation. Specific $CD8^+$ T-cells counts of less than 100 per million PBMCs were considered negative.

RESULTS

In the present study, we used eight Burmese rhesus macaques consisting of four animals possessing MHC-I haplotype *90-010-Ie*, two possessing *89-075-Iw*, and two possessing *91-010-Is*. After a SIVmac239 challenge, all these animals failed to control viral replication and had high set-point plasma viral loads (geometric mean: 3×10^5 copies/mL) (Fig. 1).

We examined SIV-specific $CD8^+$ T cell responses at week 2 and week 6 or 12 after SIV challenge in these animals by detection of specific IFN-γ induction after stimulation using peptide mixtures (Figs. 2 and 3). At week 6 or 12, we examined $CD8^+$ T cell responses specific for the N-terminal half of Gag (Gag-N), the C-terminal half of Gag (Gag-C), Vif, Nef, the N-terminal half of Pol (Pol-N), the C-terminal half of Pol (Pol-C), Vpx, Vpr, the N-terminal half of Env (Env-N), the C-terminal half of Env (Env-C), Tat, and Rev. At week 2, however, we examined only Gag-N-, Gag-C-, Vif- and Nef-specific $CD8^+$ T cell responses because of limited availability of PBMCs.

In the first group of macaques, which possessed *90-010-Ie*, neither Gag- nor Vif-specific $CD8^+$ T cell responses were induced efficiently at week 2 (Fig. 2). Even at week 12, these responses were undetectable in most of the animals. In contrast, Nef-specific $CD8^+$ T cell responses were detected at week 2, 6, or 12 in all four animals. Env-specific $CD8^+$ T cell responses were detectable at week 12 in three of them. These results indicate that, during primary SIV infection in *90-010-Ie*-positive macaques, Gag- or Vif-specific $CD8^+$ T cell responses are not induced, however Nef-specific $CD8^+$ T cell responses are.

In the second group of macaques, which possessed *89-075-Iw*, Gag- and Vif-specific $CD8^+$ T cell responses were elicited efficiently (Fig. 3a). In the third group of macaques, which possessed *91-010-Is*, Gag-, Vif- and Nef-specific $CD8^+$ T cell responses were elicited efficiently (Fig. 3b). Other SIV antigen-specific $CD8^+$ T cell responses were not efficiently induced in these two groups except for Tat-specific $CD8^+$ T cell responses in macaque

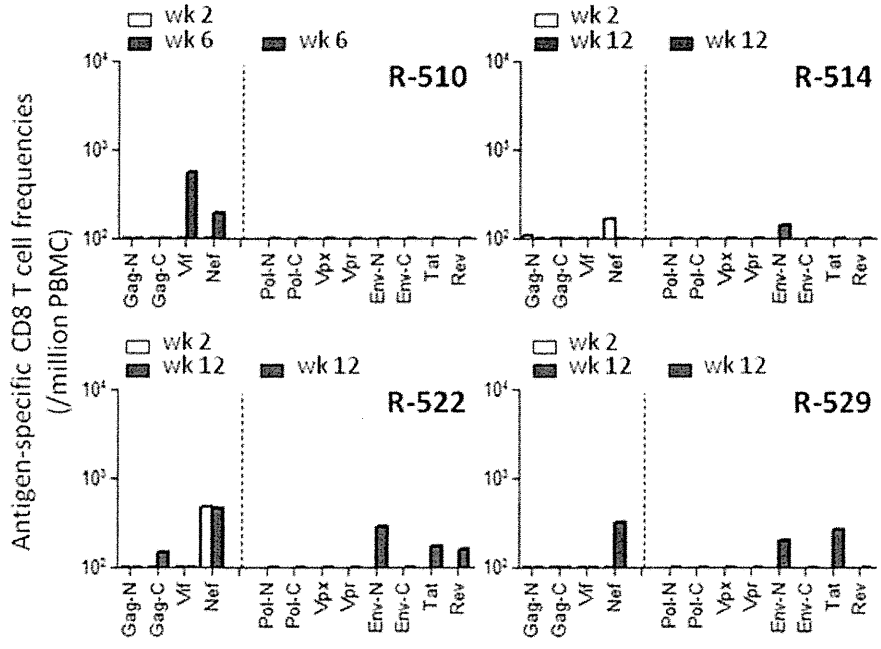

Fig. 2. SIV antigen-specific $CD8^+$ T cell frequencies in the first group of macaques, which possessed *90-010-Ie*. Gag-, Vif- and Nef-specific $CD8^+$ T cell frequencies at week 2 and Gag-, Vif-, Nef-, Pol-, Vpx-, Vpr-, Env-, Tat- and Rev-specific $CD8^+$ T cell frequencies at weeks 6 or 12 are shown.

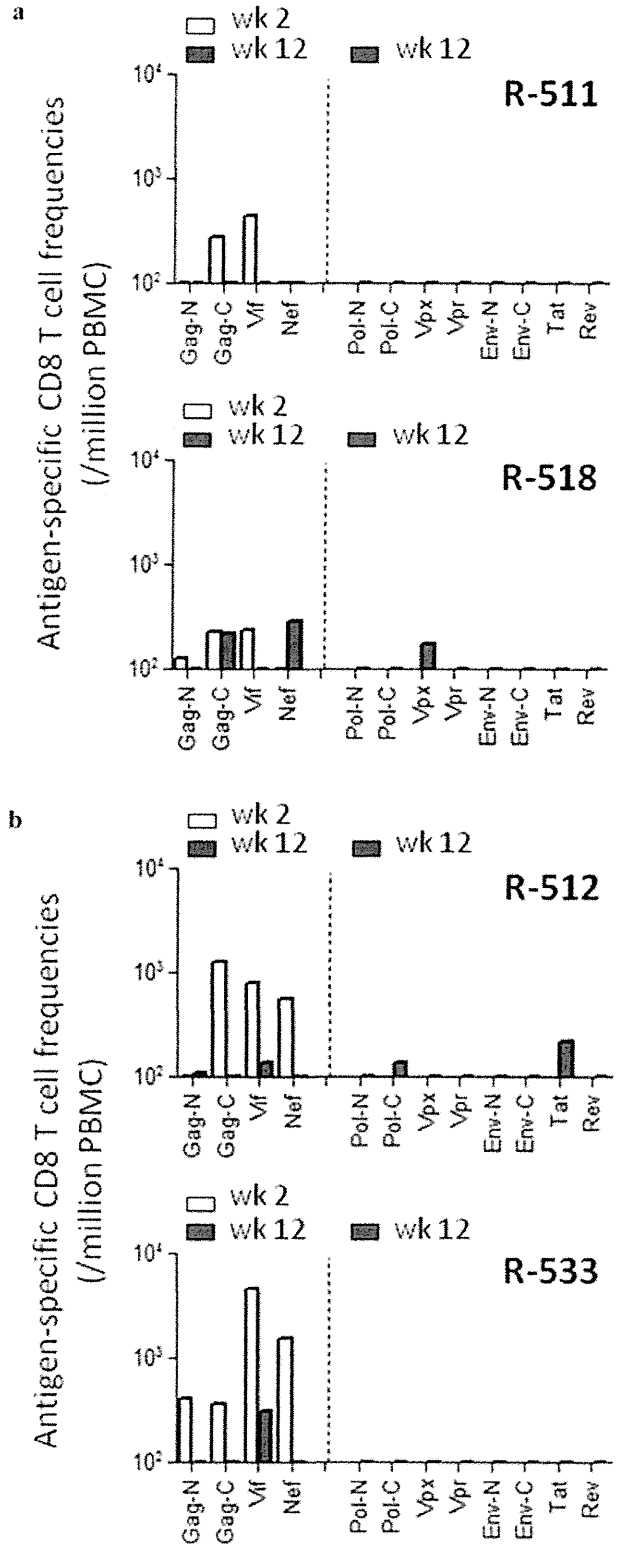

Fig. 3. SIV antigen-specific CD8$^+$ T cell frequencies in (a) the second group of macaques, which possessed *89-075-Iw* and (b) the third, which possessed *91-010-Is*.

R-512. Thus, in the four animals possessing *89-075-Iw* or *91-010-Is*, Gag- or Vif-specific CD8$^+$ T cell responses were induced more efficiently than Nef-specific ones at week 2. These responses in PBMCs were mostly diminished at week 12; possibly reflecting the considerable CTL consumption in the effector sites in animals with high viral loads.

DISCUSSION

Previous studies have indicated the potential of Gag-specific CTL responses to suppress HIV/SIV replication *in vivo* (12, 13, 16). Further, our recent study suggested the potency of Vif-specific CTL responses (17). Then, in the present study, we examined Gag- and Vif-specific CTL responses during primary SIV infection in three groups of animals, each group having a different MHC-I haplotype. Although the numbers of CTL frequencies differed between groups, the CTL responses tended have similar patterns.

Our previous study showed vaccine efficacy in a group of macaques with the MHC-I haplotype *90-120-Ia* (15, 16). Unvaccinated *90-120-Ia*-positive macaques predominantly induce Gag-specific CTL responses but fail to control viremia, while vaccinated ones show enhanced Gag-specific CTL responses and control SIV replication. $Gag_{206–216}$ epitope-specific and $Gag_{241–249}$ epitope-specific CTL responses were shown to be responsible for this vaccine-based viral control (16). However, some Gag-specific CTLs may be effective while others are not. Further analysis of this type of vaccine efficacy would contribute to understanding the requisites for vaccine-based viral control. Possibly, the *89-075-Iw*-positive or *91-010-Is*-positive animals presented in this study may be a candidate model for such analysis.

In primary SIVmac239 infection, it is speculated that some MHC-I haplotypes (referred to as type 1) are associated with Gag/Vif-specific CTL responses while others (referred to as type 2) are not. The MHC-I haplotype *90-120-Ia* described above belongs to type 1. In the present study, the second group, which possess MHC-I haplotype *89-075-Iw*, and the third, which possess *91-010-Is*, both showed efficient Gag- and Vif-specific CTL responses in primary SIV infection, although it remains undetermined whether these MHC-I haplotypes belong to type 1. In contrast, the first group of macaques, which possess MHC-I haplotype *90-010-Ie* did not show efficient Gag- or Vif-specific CTL responses in primary SIV infection. Instead, Nef-specific CTL responses were induced in all four animals. This suggests that the MHC-I haplotype *90-010-Ie* belongs to type 2; that is, primary SIV infection induces no predominant CTL responses specific for Gag/Vif epitopes

restricted by *90-010-Ie*-derived MHC-I molecules. Our results imply that CTLs exerted selective pressure on SIV *gag* and *vif* in the second/third groups but not in the first group. Larger number of animals would enable us to compare those with type 1 and 2 MHC-I haplotypes, which would contribute to our understanding of the efficacy of Gag- and Vif-specific CTL responses against SIV infection.

In developing a prophylactic CTL-inducing AIDS vaccine, it would be important to induce CTL memory resulting in potent CTL responses post-HIV exposure, while prophylactic vaccination can affect the immunodominance patterns of CTL responses post-viral exposure (23, 24). Gag- and Vif-specific CTL memory induction may be a promising vaccine strategy, but the influence of prophylactic vaccination on the patterns of CTL responses post-viral exposure would be affected by MHC-I genotypes. In the hosts in which Gag- and Vif-specific CTL responses are induced during the natural course of SIV infection, Gag- and Vif-specific CTL memory induction by prophylactic vaccination would predominantly enhance these CTL responses. In contrast, in those in whom no Gag- or Vif-specific CTL responses occurred during the natural course of SIV infection, prophylactic vaccination inducing Gag- and Vif-specific CTL responses would result in broader CTL responses. Macaques in which both MHC-I haplotypes belong to type 2 may be ideal for evaluation of this type of vaccine efficacy, but it is very difficult to accumulate those animals. It would be reasonable to use groups of macaques possessing type 2 haplotypes such as the group 1 (*90-010-Ie*-positive macaques) presented in this study for such evaluation.

In summary, by focusing on Gag- and Vif-specific CTL responses, we found two types of rhesus macaques that showed different patterns of CTL responses during primary SIV infection; one elicited Gag- and Vif-specific CTL responses but the other did not. Accumulated analyses in both types of animals would contribute to understanding the impact of these potent CTL responses on primary SIV infection.

ACKNOWLEDGMENTS

This work was supported by grants-in-aid from the Ministry of Education, Culture, Sports, Science, and Technology, grants-in-aid from the Ministry of Health, Labor, and Welfare, and a grant from Takeda Science Foundation in Japan.

REFERENCES

1. Koup R.A., Safrit J.T., Cao Y., Andrews C.A., McLeod G., Borkowsky W., Farthing C., Ho D.D. (1994) Temporal association of cellular immune responses with the initial control of viremia in primary human immunodeficiency virus type 1 syndrome. *J Virol* **68:** 4650–55.
2. Borrow P., Lewicki H., Hahn B.H., Shaw G.M., Oldstone M.B. (1994) Virus-specific CD8+ cytotoxic T-lymphocyte activity associated with control of viremia in primary human immunodeficiency virus type 1 infection. *J Virol* **68:** 6103–10.
3. Matano T., Shibata R., Siemon C., Connors M., Lane H.C., Martin M.A. (1998) Administration of an anti-CD8 monoclonal antibody interferes with the clearance of chimeric simian/human immunodeficiency virus during primary infections of rhesus macaques. *J Virol* **72:** 164–9.
4. Jin X., Bauer D.E., Tuttleton S.E., Lewin S., Gettie A., Blanchard J., Irwin C.E., Safrit J.T., Mittler J., Weinberger L., Kostrikis L.G., Zhang L., Perelson A.S., Ho D.D. (1999) Dramatic rise in plasma viremia after CD8(+) T cell depletion in simian immunodeficiency virus-infected macaques. *J Exp Med* **189:** 991–8.
5. Goulder P.J., Watkins D.I. (2004) HIV and SIV CTL escape: implications for vaccine design. *Nat Rev Immunol* **4:** 630–40.
6. Kaslow R.A., Carrington M., Apple R., Park L., Munoz A., Saah A.J., Goedert J.J., Winkler C., O'Brien S.J., Rinaldo C., Detels R., Blattner W., Phair J., Erlich H., Mann D.L. (1996) Influence of combinations of human major histocompatibility complex genes on the course of HIV-1 infection. *Nat Med* **2:** 405–11.
7. Tang J., Tang S., Lobashevsky E., Myracle A.D., Fideli U., Aldrovandi G., Allen S., Musonda R., Kaslow R.A. (2002) Favorable and unfavorable HLA class I alleles and haplotypes in Zambians predominantly infected with clade C human immunodeficiency virus type 1. *J Virol* **76:** 8276–84.
8. Goulder P.J., Watkins D.I. (2008) Impact of MHC class I diversity on immune control of immunodeficiency virus replication. *Nat Rev Immunol* **8:** 619–30.
9. Migueles S.A., Sabbaghian M.S., Shupert W.L., Bettinotti M.P., Marincola F.M., Martino L., Hallahan C.W., Selig S.M., Schwartz D., Sullivan J., Connors M. (2000) HLA B*5701 is highly associated with restriction of virus replication in a subgroup of HIV-infected long term nonprogressors. *Proc Natl Acad Sci USA* **97:** 2709–14.
10. Altfeld M., Addo M.M., Rosenberg E.S., Hecht F.M., Lee P.K., Vogel M., Yu X.G., Draenert R., Johnston M.N., Strick D., Allen T.M., Feeney M.E., Kahn J.O., Sekaly R.P., Levy J.A., Rockstroh J.K., Goulder P.J., Walker B.D. (2003) Influence of HLA-B57 on clinical presentation and viral control during acute HIV-1 infection. *AIDS* **17:** 2581–91.
11. Yant L.J., Friedrich T.C., Johnson R.C., May G.E., Maness N.J., Enz A.M., Lifson J.D., O'Connor D.H., Carrington M., Watkins D.I. (2006) The high-frequency major histocompatibility complex class I allele Mamu-B*17 is associated with control of simian immunodeficiency virus SIVmac239 replication. *J Virol* **80:** 5074–7.
12. Kiepiela P., Ngumbela K., Thobakgale C., Ramduth D., Honeyborne I., Moodley E., Reddy S., de Pierres C., Mncube Z., Mkhwanazi N., Bishop K., van der Stok M., Nair K., Khan N., Crawford H., Payne R., Leslie A., Prado J., Prendergast A., Frater J., McCarthy N., Brander C., Learn G.H., Nickle D., Rousseau C., Coovadia H., Mullins J.I., Heckerman D., Walker B.D., Goulder P. (2007) CD8+ T-cell responses to different HIV proteins have discordant associations with viral load. *Nat Med* **13:** 46–53.
13. Sacha J.B., Chung C., Rakasz E.G., Spencer S.P., Jonas A.K., Bean A.T., Lee W., Burwitz B.J., Stephany J.J., Loffredo J.T., Allison D.B., Adnan S., Hoji A., Wilson N.A., Friedrich T.C., Lifson J.D., Yang O.O., Watkins D.I. (2007) Gag-specific $CD8^+$ T lymphocytes recognize infected cells before AIDS-virus integration and viral protein expression. *J Immunol* **178:** 2746–54.
14. Matano T., Kano M., Nakamura H., Takeda A, Nagai Y. (2001) Rapid appearance of secondary immune responses and protection from acute CD4 depletion after a highly pathogenic

immunodeficiency virus challenge in macaques vaccinated with a DNA prime/Sendai virus vector boost regimen. *J Virol* **75:** 11891–6.
15. Matano T., Kobayashi M., Igarashi H., Takeda A., Nakamura H., Kano M., Sugimoto C., Mori K., Iida A., Hirata T., Hasegawa M., Yuasa T., Miyazawa M., Takahashi Y., Yasunami M., Kimura A., O'Connor D.H., Watkins D.I., Nagai Y. (2004) Cytotoxic T lymphocyte-based control of simian immunodeficiency virus replication in a preclinical AIDS vaccine trial. *J Exp Med* **199:** 1709–18.
16. Kawada M., Tsukamoto T., Yamamoto H., Iwamoto N., Kurihara K., Takeda A., Moriya C., Takeuchi H., Akari H., Matano T. (2008) Gag-specific cytotoxic T-lymphocyte-based control of primary simian immunodeficiency virus replication in a vaccine trial. *J Virol* **82:** 10199–206.
17. Iwamoto N., Tsukamoto T., Kawada M., Takeda A., Yamamoto H., Takeuchi H., Matano T. (2010) Broadening of $CD8^+$ cell responses in vaccine-based simian immunodeficiency virus controllers. *AIDS* **24:** 2777–87.
18. Loffredo J.T., Bean A.T., Beal D.R., Leon E.J., May G.E., Piaskowski S.M., Furlott J.R., Reed J., Musani S.K., Rakasz E.G., Friedrich T.C., Wilson N.A., Allison D.B., Watkins D.I. (2008) Patterns of CD8+ immunodominance may influence the ability of Mamu-B*08-positive macaques to naturally control simian immunodeficiency virus SIVmac239 replication. *J Virol* **82:** 1723–38.
19. Tenzer S., Wee E., Burgevin A., Stewart-Jones G., Friis L., Lamberth K., Chang C.H., Harndahl M., Weimershaus M., Gerstoft J., Akkad N., Klenerman P., Fugger L., Jones E.Y., McMichael A.J., Buus S., Schild H., van Endert P., Iversen A.K. (2009) Antigen processing influences HIV-specific cytotoxic T lymphocyte immunodominance. *Nat Immunol* **10:** 636–46.
20. Takahashi-Tanaka Y., Yasunami M., Naruse T., Hinohara K., Matano T., Mori K., Miysazawa M., Honda M., Yasutomi Y., Nagai Y., Kimura A. (2007) Reference strand-mediated conformation analysis (RSCA)-based typing of multiple alleles in the rhesus macaque MHC class I Mamu-A and Mamu-B loci. *Electrophoresis* **28:** 918–24.
21. Naruse T.K., Chen Z., Yanagida R., Yamashita T., Saito Y., Mori K., Akari H., Yasutomi Y., Miyazawa M., Matano T., Kimura A. (2010) Diversity of MHC class I genes in Burmese-origin rhesus macaques. *Immunogenetics* **62:** 601–11.
22. Kestler H.W. 3rd, Ringler D.J., Mori K., Panicali D.L., Sehgal P.K., Daniel M.D., Desrosiers R.C. (1991) Importance of the nef gene for maintenance of high virus loads and for development of AIDS. *Cell* **65:** 651–62.
23. Tsukamoto T., Takeda A., Yamamoto T., Yamamoto H., Kawada M., Matano, T. (2009) Impact of cytotoxic-T-lymphocyte memory induction without virus-specific CD4+ T-cell help on control of a simian immunodeficiency virus challenge in rhesus macaques. *J Virol* **83:** 9339–46.
24. Takahara Y., Matsuoka S., Kuwano T., Tsukamoto T., Yamamoto H., Ishii H., Nakasone T., Takeda A., Inoue M., Iida A., Hara H., Shu T., Hasegawa M., Sakawaki H., Horiike M., Miura T., Igarashi T., Naruse T.K., Kimura A., Matano T. (2011) Dominant induction of vaccine antigen-specific cytotoxic T lymphocyte responses after simian immunodeficiency virus challenge. *Biochem Biophys Res Commun* Epub ahead of print.

Virology 423 (2012) 107–118

Contents lists available at SciVerse ScienceDirect

Virology

journal homepage: www.elsevier.com/locate/yviro

Lymph nodes harbor viral reservoirs that cause rebound of plasma viremia in SIV-infected macaques upon cessation of combined antiretroviral therapy

Mariko Horiike [a], Shingo Iwami [a,b,c], Makoto Kodama [d], Akihiko Sato [d], Yuji Watanabe [a], Mika Yasui [a], Yuki Ishida [a], Takeshi Kobayashi [a], Tomoyuki Miura [a], Tatsuhiko Igarashi [a,*]

[a] Laboratory of Primate Model, Experimental Research Center for Infectious Diseases, Institute for Virus Research, Kyoto University, Kyoto 606-8507, Japan
[b] Precursory Research for Embryonic Science and Technology (PRESTO), Japan Science and Technology Agency (JST), Kawaguchi, Saitama 332-0012, Japan
[c] Graduate School of Mathematical Sciences, The University of Tokyo, Meguro-ku, Tokyo 153-8914, Japan
[d] Medical Research Laboratories, Shionogi & Co. Ltd., Osaka 566-0022, Japan

ARTICLE INFO

Article history:
Received 27 September 2011
Returned to author for revision
6 November 2011
Accepted 29 November 2011
Available online 21 December 2011

Keywords:
SIV
Antiretroviral therapy
HIV-1
HAART
Rebound of plasma viremia
Reservoirs
Animal model

ABSTRACT

Attempts to find a cure for HIV infection are hindered by the presence of viral reservoirs that resist highly active antiretroviral therapy. To identify the properties of these reservoirs, four SIV239-infected Rhesus macaques were treated with combined antiretroviral therapy (cART) for 1 year. While plasma viral RNA (vRNA) was effectively suppressed, a systemic analysis revealed that vRNA was distributed in the following order: lymphatic tissues > lungs and intestine > other tissues. Histochemistry yielded no cells with viral signals. To increase the chance of detection, two additional SIV-infected animals were treated and analyzed on Day 10 after the cessation of cART. These animals exhibited similar vRNA distribution patterns to the former animals, and immunohistochemistry revealed Nef-positive T lymphocytes predominantly in the follicles of mesenteric lymph nodes (MLNs). These data suggest that lymphatic tissues, including MLNs, contain major cellular reservoirs that cause rebound of plasma viremia upon cessation of therapy.

Introduction

Highly active antiretroviral therapy (HAART), which consists of three or more anti-HIV-1 drugs, is currently the primary choice of therapeutic intervention for HIV-1-infected individuals (Department of Health and Human Services (DHHS), 2011). The circulating viral loads in these patients are, in most cases, effectively suppressed below the limit of detection (<50 copies/ml of plasma) by HAART (Richman, 2001). However, the virus loads promptly rebound to pretreatment levels upon cessation of HAART (Chun et al., 1999), which suggests the persistence of viral reservoirs during the combined antiviral therapy. Therefore, to achieve a complete cure of HIV-1 infection, it is essential to eradicate these viral reservoirs.

Resting $CD4^+$ T lymphocytes have been identified as a viral reservoir (Chun et al., 1997; Finzi et al., 1997; Wong et al., 1997). These cells harbor intact viral genomes integrated into their chromosomes and produce infectious virus particles when they are reactivated in response to stimulation. It is noteworthy that the estimated half-life of a resting $CD4^+$ T cell is more than 44 months (Siliciano et al., 2003), which provides a theoretical basis for the source of the virus that rebounds upon cessation of long-term, successful HAART. Resting $CD4^+$ T lymphocyte is probably not the only reservoir of HIV-1. In the majority of patients on HAART, the rebounding viral genotypes detected in the plasma upon cessation of therapy were dissimilar to the genotypes extracted from resting $CD4^+$ T cells or from virus particles recovered from cells that were collected before interruption of the therapy (Chun et al., 2000).

Follicular dendritic cells (FDCs) have also been proposed as a viral reservoir (Spiegel et al., 1992). These cells are present in the follicles formed in all secondary lymphoid tissue. Rather than being infected with virus, FDCs retain infectious HIV-1 particles on the cell surface and transfer them to $CD4^+$ T lymphocytes (Burton et al., 2002). Since FDCs retain numerous virus particles, the genomes of which exhibit greater diversity than those in other tissues or cells and which reportedly hold infectious particles for months to years, it seems likely that these cells serve as archives of infectious virions (Keele et al., 2008).

The recently developed method for ultrasensitive detection of plasma viral burdens has revealed that patients who have HAART-controlled viremia (below the detection limit by clinical criteria; i.e., <50 copies/ml plasma) over several years still harbor minuscule

* Corresponding author at: Room 301, Molecular Biology Research Bldg, Institute for Virus Research, Kyoto University, 53 Kawahara-cho, Shogoin, Sakyo ward, Kyoto, Kyoto 606-8507, Japan. Fax: +81 75 761 9335.
E-mail address: tigarash@virus.kyoto-u.ac.jp (T. Igarashi).

0042-6822/$ – see front matter © 2011 Elsevier Inc. All rights reserved.
doi:10.1016/j.virol.2011.11.024

amounts of virion-associated RNA in the circulation (Palmer et al., 2008), suggesting ongoing viral replication, i.e., "residual viremia". The potential for ongoing HIV-1 replication during HAART is supported by evidence of *env* gene evolution in patients receiving HAART (Frost et al., 2001; Martinez et al., 1999), as well as the detection in patients on HAART of 1-LTR and 2-LTR circles, episomal HIV-1 cDNAs, the presence of which most likely reflects recent infection (Sharkey et al., 2000, 2005). A transient increase in the number of 2-LTR circles, probably reflecting an increase in the number of failed attempts to integrate into the host cell genome, was detected in approximately 30% of infected individuals who were receiving HAART, when an integrase inhibitor was added as treatment intensification (Buzon et al., 2010). Based on these lines of evidence, it is conceivable that certain cell types, as yet to be identified, allow productive replication of HIV-1 during HAART. Although HAART theoretically arrests *de novo* virus replication, these unidentified reservoirs appear to be refractory to the antiviral effects of the regimen through unknown mechanisms.

It is postulated that viral reservoirs in the host retain HIV-1 during HAART as follows: resting $CD4^+$ T lymphocytes store inducible viral genomes, FDCs archive infectious particles, and unidentified cells support productive viral replication cycles. It remains to be revealed whether other cell types serve as viral reservoirs using other mechanisms, and which cell type is the most important for sequestering HIV-1.

Peripheral blood samples from volunteer patients have been used in studies to identity HIV-1 reservoirs (Brennan et al., 2009; Chun et al., 2000; Sharkey et al., 2011). However, HIV-1 predominantly replicates in $CD4^+$ T lymphocytes in the lymphoid tissues (Embretson et al., 1993; Pantaleo et al., 1993), particularly the intestine, which is home to 70–90% of all lymphocytes in the body and which is severely affected during the acute phase of infection (Brenchley et al., 2004; Guadalupe et al., 2003), determining prognosis. Therefore a systemic analysis, in addition to existing studies on peripheral blood, would elucidate the mechanisms underlying rebound of plasma viremia upon discontinuation of HAART. Since it is unethical to collect various tissues from patients for analysis, an alternative model system is required. In this regard, the SIV/macaque model, which has been useful in understanding HIV-1 infection, is suitable for investigations of viral reservoirs using a systemic analysis (Dinoso et al., 2009; North et al., 2009).

Using the SIV239/macaque system, we investigated HIV-1 reservoirs during combined antiviral therapy (cART). First, we conducted a systemic analysis of SIV-infected Rhesus macaques that received cART for an extended period. SIV239 has been extensively used as a tractable animal model for HIV-1 in studies of replication, pathogenesis, and vaccine development. In addition, this virus causes almost complete depletion of $CD4^+$ T lymphocytes in the intestine (Veazey et al., 1998), as HIV-1 does in patients who suffer from AIDS.

Results

Establishment of anti-SIV239 cART regimen with oral administration

Before the experimental infection of macaques with SIV, we established an antiretroviral regimen that is applicable to SIV239 infection in the Rhesus macaque model. Given that NNRTIs do not suppress replication of SIV (Balzarini et al., 1995), anti-HIV-1 drugs belonging to this class were excluded from consideration. Regarding NRTIs, several studies have confirmed that Tenofovir (TDF) and its pro-drug PMPA are effective against SIV. Some studies have used Zidovudine (AZT) and Lamivudine (3TC) to suppress SIV replication *in vitro* and *in vivo* (Balzarini et al., 1995; Benlhassan-Chahour et al., 2003). Based on the results of these studies, we included TDF (Viread) and AZT/3TC (Combivir) in our regimen. Regarding protease inhibitors (PIs), Saquinavir (SQV) has been shown to be effective against SIV *in vitro* (Giuffre et al., 2003; Witvrouw et al., 2004). When we initiated this study, the anti-SIV efficacies of other commercially available PIs had not yet been reported. To determine which PI to include in our cART, we examined three commercially available PIs – SQV, Lopinavir/Ritonavir (LPV/RTV; Kaletra), and Atazanavir (ATV; Reyataz) – in the MT-4/MTT assay. This assay, which was originally developed to measure cell proliferation, was used to evaluate inhibition of virus-induced killing of human T-lymphoid MT-4 cells in the presence of increasing amounts of the drugs (Pauwels et al., 1988). Along with SIV239, HIV-1 IIIB was employed in the assay as a control. All of the compounds tested suppressed the activity of SIV239. The EC_{50} values for SQV were 18.5 nM against SIV and 22.7 nM against HIV-1 (Table 1 and Supplemental Fig. 1). The EC_{50} ratio, i.e., the EC_{50} value against SIV divided by the EC_{50} value against HIV-1, was 0.8 (Table 1). The EC_{50}s against SIV239 and the EC50 ratios of the other two drugs were: 52.2 nM and 1.5, respectively, for LPV/RTV; and 80.0 nM and 4.7, respectively, for ATV. Pharmacokinetic information on these drugs is available, and the half-life in the circulation in humans is: 1–2 h for SQV; 5–6 h for LPV/RTV; and 7 h for ATV (Department of Health and Human Services (DHHS), 2011). Taking into account the EC_{50}, the half-life (which defines the required frequency of administration to maintain the drug level), and cost-effectiveness, we included LPV/RTV in our regimen.

Drug administration was instituted *per os*, to effectively model the metabolism and pharmacokinetics of the antiviral drugs in patients. The dosage and administration of these drugs are described in the Materials and methods section. To assess whether a given dosage resulted in a measurable concentration of the drug in the circulation even after a long interval, blood samples were collected from six monkeys at 14 h after intake and the antiviral effect in plasma was determined by titration. The drug concentrations in the animals' blood ranged from 7.2 to 29.5 μM (LPV/RTV equivalent); these levels are 5- to 20-fold higher than those recommended for adult patients (1.5 μM for LPV/RTV equivalent) (Department of Health and Human Services (DHHS), 2011). Plasma samples from two representative animals, which had already been measured in the biological assay, were also subjected to HPLC. The results of the HPLC analysis revealed drug concentrations comparable to those determined by the biological assay: 16.1 μM for one animal (20.0 μM by the MTT assay) and 25.7 μM for the other animal (24.8 μM by the MTT assay), thus justifying our use of the biological assay to measure levels of antiviral activity in the circulation of SIV-infected animals during therapy. Based on these results, we finalized the regimen.

Efficacy of the cART regimen for macaques infected with SIV239

The establishment of the anti-SIV regimen enabled us to conduct animal experiments. Seven Rhesus macaques were inoculated intravenously with 2000 $TCID_{50}$ of the SIV239 virus stock. All animals exhibited an initial peak of viremia at 2 weeks post-inoculation (pi) (median, 2.2×10^7 copies/ml; range, $7.9–60.0\times10^6$ copies/ml, Fig. 1). At 8 weeks pi, when the viral loads decreased from the initial peak and plateaued (median, 1.3×10^5 copies/ml; range, $1.1–4.9\times10^5$ copies/ml), the cART was

Table 1
Efficacies of commercially available anti-HIV-1 protease inhibitors against SIV239 and HIV-1 IIIB.

Compounds	EC_{50}[a] (nM)		EC_{50} ratio[b]
	SIV239	HIV-1 IIIB	
Saquinavir	18.5	22.7	0.8
Lopinavir/ritonavir	52.2	35.6	1.5
Atazanavir	80.0	16.9	4.7

[a] 50% effective concentration.
[b] EC_{50} value against SIV239 divided by the EC_{50} value against HIV-1 IIIB.

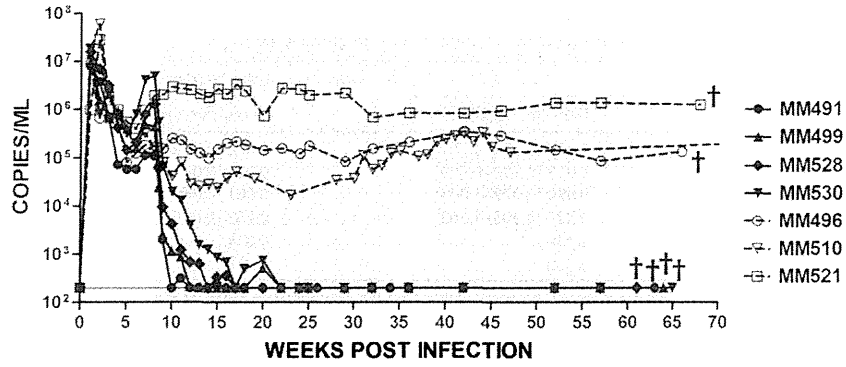

Fig. 1. Effects of cART on plasma viral loads. Seven Rhesus macaques were inoculated with SIV239. Four animals, MM491, MM499, MM528, and MM530 (solid lines), were treated with cART (shaded areas). Animals MM510, MM496, and MM521 (dotted line) served as untreated controls. The detection limit of our RT-PCR assay is 200 RNA copies/ml, and samples with levels below the level of detection are plotted as 200 RNA copies/ml. †, time of euthanasia.

administered to four of the monkeys (MM491, MM499, MM528, and MM530; designated as group A).

Upon drug administration, the plasma viral RNA (vRNA) levels in these animals promptly started to decrease. There was an inverse inclination between set point plasma vRNA load and duration to suppress vRNA to the detection limit (200 copies/ml). The vRNA of MM491, whose set point viral RNA level was the lowest in the group 1.1×10^5 copies/ml, fell below the detection limit in 2 weeks. MM499 and MM528, whose plasma vRNAs were 4.4×10^5 and 1.3×10^6 copies/ml at the initiation of cART, took 5 and 6 weeks, respectively. After nine weeks of treatment, the viral burden of MM530, which had the highest level in the group at 4.9×10^6 copies/ml, was undetectable. Plasma vRNA levels of all animals on cART had fallen below the limit of detection by 17 weeks pi. When HAART was applied to SIV/pigtailed macaque or RT-SHIV/rhesus macaque models, it took 8 and 18 weeks, respectively, to suppress circulating vRNA to below the detection limit (Dinoso et al., 2009; North et al., 2009). When considering variables from previous studies, including virus strain, drug combinations, detection limit of vRNA measurement, and initiation of treatment of these studies, it is conceivable that the cART approach devised in the current study is as potent in terms of the progress to viral containment.

To relate our results to previous studies on vRNA declines for HIV-1 and SIV following antiviral therapy, we examined the levels of viremia in our infected monkeys during the first few weeks after the initiation of therapy (Table 2 and Supplemental Fig. 2). Each individual monkey followed a similar pattern of viral decay: an initial rapid and exponential reduction by almost 2.5 orders of magnitude (comprising the first phase, which is presumably associated with short-lived infected cells), followed by a slower exponential decline of 1.5 orders of magnitude (the second phase, which is presumably associated with long-lived infected cells). The observed biphasic decay of viral burdens was consistent with previous findings from studies on SIV models and patients with HIV-1 (Dinoso et al., 2009; Murray et al., 2007; Perelson et al., 1997; Perelson and Nelson, 1999). Decay rates for the first and second phases were deduced by employing mathematical modeling (Table 2). The decay rates of the first phase ranged from 0.495 (for MM491) to 0.853 (for MM499), and those of the second phase ranged from 0.028 (for MM491) to 0.089 (for MM499). The decay rates of plasma vRNA loads during the first phase in patients with HIV-1 on HAART, consisting of LPV/RTV, Efavirenz, 3TC, and TDF, exhibited comparable numbers to those in the current study, ranging from 0.6 to 1.4 (Markowitz et al., 2003). Mean half-lives of ($\log 2/a=$) 1.13 for the first phase and ($\log 2/\mu_M$) 14.24 days for the second phase were comparable to those observed in patients with HIV-1 on HAART. Half-lives of HIV-1 RNA in the circulation of HIV-1-infected patients on suppressive ART, consisting of Indinavir and Efavirenz, ranged from 0.6 to 2.0 days for the first phase and 5.2 to 35.6 days for the second phase (Havlir et al., 2003). Comparison of the viral decay rates derived in the current study with those derived in previous reports (Perelson et al., 1997) gave statistically insignificant results ($P=0.667$ for the first phase, and $P=0.662$ for the second phase). These results suggest that the virologic response of SIV infected Rhesus macaques to cART, as reported in a recent study (Dinoso et al., 2009), is comparable to the response of HIV-1-infected patients to HAART.

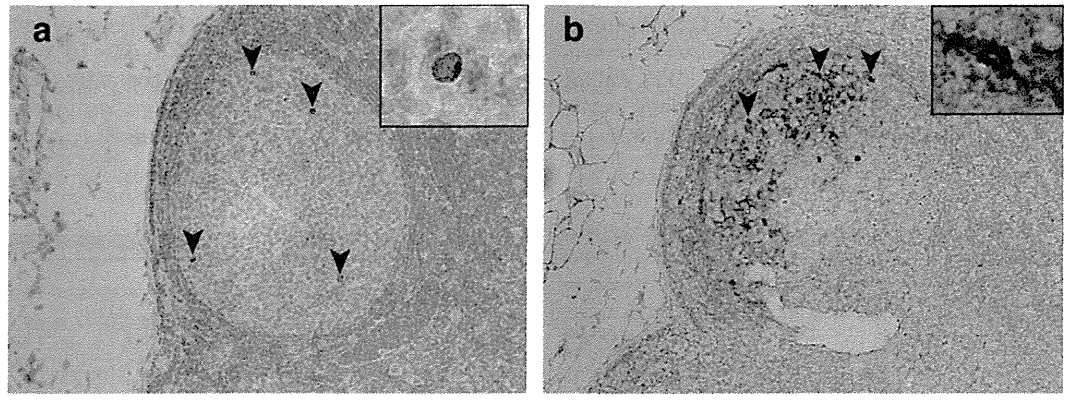

Fig. 2. Nef-expressing cells detected in the iMLNs of animal MM511. (a) The section was stained with the anti-SIV Nef mouse monoclonal antibody. (b) Juxtaposition of Nef-expressing cells and CD35-positive FDCs in the follicle of an iMLN from MM511. The sample was stained using the anti-SIV Nef mouse monoclonal antibody (brown) and the anti-CD35 mouse monoclonal antibody (blue). Original magnification, ×40. The insets contain a higher-magnification, ×126 equivalent (original magnification, ×63).

Table 2
Decay rate and half-life derived by mathematical modeling of short- or long-lived infected cells in group A monkeys.

Animal ID	Short-lived infected cells		Long-lived infected cells	
	Decay rate : a (day^{-1})	Half-life : $log2/a$ (days)	Decay rate : μ_M (day^{-1})	Half-life : $log2/\mu_M$ (days)
MM491	0.495 [0.405–0.605][a]	1.400 [1.146–1.711]	0.028 [0.000–0.141]	24.76 [4.916–∞]
MM499	0.853 [0.807–1.287]	0.813 [0.539–0.859]	0.089 [0.083–0.100]	7.753 [6.931–8.402]
MM528	0.707 [0.661–0.746]	0.980 [0.929–1.049]	0.061 [0.045–0.070]	11.44 [9.846–15.44]
MM530	0.523 [0.372–0.575]	1.325 [1.205–1.863]	0.053 [0.035–0.064]	13.00 [10.85–19.86]
Mean	0.645	1.130	0.058	14.24
S.D.	0.168	0.279	0.025	7.351

[a] Values in parentheses represent the lower and upper 68% confidence intervals, calculated by a bootstrap method in which each experiment was simulated 1000 times.

Patients with HIV-1 on HAART exhibit undetectable levels of plasma vRNA (typically less than 50 copies/ml) when the therapy works as expected. To estimate suppression levels achieved by the regimen used in the current study, selected plasma samples with adequate volume from animals in group A were subjected to another quantitative real-time PCR assay with a lower detection limit. Using 1.5-ml plasma samples, which were collected at 29, 42, and 52 weeks pi, and at euthanasia, particle-associated vRNA was extracted and amplified. All of these samples yielded less than 20 copies/ml of vRNA loads (Table 3), except for those collected at 42 and 52 weeks pi (44 and 47 copies/ml, respectively) from MM530, which exhibited the highest plasma vRNA at the start of cART (4.9×10^6 copies/ml) and required the longest duration to suppress vRNA to 200 copies/ml (9 weeks). These results confirm that the regimen established in the current study is as suppressive as those applied to patients. Based on the progression to viral containment, decay rates, and suppression levels, we concluded that the cART established in the current study is comparable to therapies used to treat patients with HIV-1 and suitable to pursue viral reservoirs during therapy. The suppressed viral burdens of the treated animals were maintained below the limit of detection throughout the course of treatment (up to 52 weeks). In contrast, the viral burdens of the untreated animals (MM496, MM510, and MM521) remained at $>1.0\times10^5$ copies/ml until the day of necropsy (Fig. 1). Assuming a limit of viral detection of 200 copies/ml, there was a statistically significant difference in the plasma vRNA levels between the two groups of animals at week 42 ($P<0.05$).

During the entire course of cART, the levels of antiviral activity in the plasma samples of animals MM491, MM528, and MM530 assessed by MT-4/MTT assay were above the recommended trough level for adult patients (for MM491: range, 3.5–17.8 μM LPV/RTV equivalent; for MM528: range, 6.0–24.9 μM LPV/RTV equivalent; for MM530: range, 8.2–14.2 μM LPV/RTV equivalent) (Table 4). Even in the remaining animal, MM499, in which the circulating concentration of the activity was below the recommended trough level at the two time-points tested, at 10 weeks pi and at autopsy, during the course of antiviral therapy, the plasma vRNA levels were below the limit of detection. None of the treated animals exhibited a transient surge in vRNA level during the entire course of the therapy. Certain clinical conditions are known to be side-effects of antiviral drug treatment (Department of Health and Human Services (DHHS), 2011). Among the drugs employed in the present study, TDF potentially causes renal complications (Van Rompay et al., 2004) and LPV/RTV can induce abnormal lipid metabolism. In general, no significant adverse effects were noted for the drugs employed in the present study. We conclude that the antiretroviral therapy regimen established in the current study is as effective as the combined antiretroviral therapy applied to patients with HIV.

Higher titers of vRNA were detected in the lymphoid tissues of virus-infected animals undergoing antiretroviral therapy

The establishment of an effective antiretroviral therapy regimen for SIV-infected monkeys was a prerequisite for the identification of virus reservoirs during combined antiviral therapy. To this end, we considered two important questions: 'Is virus replication maintained during the therapy?', and 'If active virus replication persists, are there particular anatomic compartments that allow preferential virus replication?'

To answer these questions, we looked for the presence of vRNA in a variety of tissues collected from animals receiving cART over a period of 1 year. Total RNA was extracted from each tissue and subjected to real-time reverse transcription (RT)-PCR. Table 5 summarizes the results of RT-PCR for four animals in group A that were subjected to analysis at the end of the 1-year cART regimen, along with a representative animal that was not given treatment (MM521); all the animals were euthanized at between 61 and 68 weeks pi. In the untreated monkey (MM521), vRNA was detected in all the tissues examined, with the exception of the brainstem. In the lymphoid tissues, higher titers of vRNA (approximately 1.0×10^8 copies/μg total RNA) were detected. In the gastrointestinal tract, lungs, and vagina, in which the resident $CD4^+$ T-lymphocyte population consists mainly of $CCR5^+$ memory cells (the preferred target of HIV-1 and SIV) (Douek et al., 2003; Meng et al., 2000; Veazey et al., 2000), the vRNA titers were approximately 1.0×10^6 copies/μg of total RNA. Lower levels of vRNA were detected in the non-lymphoid tissues (heart, liver, and kidneys) and the central nervous system (cerebrum and cerebellum).

In the group A macaques, the vRNA titers in several tissues were much lower than those found in the untreated animals. The non-lymphoid tissues and central nervous system did not contain measurable amounts of vRNA. Low levels of vRNA were detected in the effector sites, such as the intestine (up to 6.5×10^4 copies/μg total RNA), lungs, and vagina (up to 6.5×10^3 copies/μg total RNA). Statistical analysis of vRNA burdens revealed significant reductions in the jejunum and rectum of animals in group A as compared to those of

Table 3
Plasma viral loads of selected samples measured by RT-PCR with a lower detection limit (20 copies/ml) in group A animals during cART.

Animals ID	Plasma viral loads (copies/ml)			
	29 wpi	42 wpi	52 wpi	At autopsy[a]
MM491	<20	<20	<20	<20
MM499	<20	<20	<20	<20
MM528	<20	<20	<20	<20
MM530	<20	44	47	<20

[a] MM491, 63 wpi; MM499, 64 wpi; MM528, 61 wpi; MM530, 65 wpi.

Table 4
Antiretroviral activities detected in the blood of animals in group A during cART.

Animals ID	Drug concentration (μM)[a]					
	10 wpi	20 wpi	32 wpi	42 wpi	56 wpi	At autopsy[b]
MM491	3.5	15.9	12.1	17.8	7.9	5.2
MM499	0.6	2.3	4.4	11.4	1.7	0.9
MM528	16.0	24.9	6.6	7.7	6.0	9.3
MM530	9.4	12.4	8.2	14.2	11.3	11.3

[a] LPV/RTV equivalent concentration.
[b] MM491, 63 wpi; MM499, 64 wpi; MM528, 61 wpi; MM530, 65 wpi.

Table 5
Viral RNA burdens in various tissues collected from SIV-infected macaques.

Tissues	vRNA levels (copies/μg total RNA)				
	Treated with cart				Untreated
	MM491 <200 copies/ml[a]	MM499 <200 copies/ml[a]	MM528 <200 copies/ml[a]	MM530 <200 copies/ml[a]	MM521 1.2×10^6 copies/ml[a]
Non-lymphoid tissues					
Heart	< 2900	< 2900	< 2900	< 2900	3.0×10^3
Liver	< 2900	< 2900	< 2900	< 2900	8.8×10^4
Kidney	< 2900	< 2900	< 2900	<2900	2.1×10^6
CNS tissues					
Cerebrum	< 2900	< 2900	< 2900	< 2900	1.1×10^6
Cerebellum	< 2900	< 2900	< 2900	< 2900	4.5×10^3
Brain stem	< 2900	< 2900	< 2900	< 2900	< 2900
Effector sites					
Lung	4.7×10^3	4.1×10^3	<2900	< 2900	1.0×10^5
Vagina	6.5×10^3	< 2900	<2900	2.9×10^3	1.3×10^5
Jejunum	5.0×10^3	3.1×10^3	1.1×10^4	7.4×10^3	1.7×10^6
Ileum	5.2×10^3	4.0×10^3	7.7×10^3	< 2900	1.4×10^6
Colon	1.8×10^4	< 2900	6.5×10^4	8.3×10^3	2.0×10^8
Rectum	2.9×10^3	< 2900	6.0×10^3	9.9×10^3	4.7×10^6
Lymphoid tissues					
Spleen	2.6×10^4	5.0×10^3	5.4×10^3	6.2×10^3	3.4×10^8
Thymus	< 2900	< 2900	N.D.	2.0×10^5	2.9×10^4
Iliac LN	5.8×10^4	6.9×10^3	1.5×10^4	3.6×10^4	1.6×10^8
Inguinal LN	< 2900	2.4×10^4	2.4×10^4	2.3×10^5	6.9×10^7
Axillary LN	8.6×10^4	7.2×10^3	3.1×10^4	2.1×10^5	7.6×10^7
iMLN	1.0×10^5	8.8×10^4	< 2900	2.9×10^5	1.0×10^8
sMLN	1.3×10^5	5.7×10^4	3.4×10^4	2.4×10^5	2.3×10^8
Submandibular LN	6.2×10^4	2.9×10^4	1.6×10^4	5.6×10^3	3.9×10^7
Bronchial LN	1.5×10^5	5.3×10^4	3.1×10^4	3.8×10^5	1.1×10^8
Splenic LN	2.5×10^5	4.3×10^4	7.3×10^3	2.0×10^5	9.8×10^7

N.D., no data; CNS, central nervous system; LNs, lymph nodes; iMLNs, inferior mesenteric lymph nodes; sMLNs, superior mesenteric lymph nodes.
Viral RNA (vRNA) levels greater than detection limit (2900 copies/μg total RNA) are represented in bold. vRNA levels are coded in grayscale as follows: white boxes, <2900; light-gray boxes, $<1.0\times10^5$; dark-gray boxes, $<1.0\times10^7$; black boxes, $>1.0\times10^7$.
[a]Viral loads in plasma.

untreated controls ($P=0.03$), indicating that cART suppressed vRNA expression in those tissues, although incompletely. Compared to the above-mentioned tissues, higher levels of vRNA (approximately 1.0×10^5 copies/μg of total RNA) were detected in the lymphoid tissues. Of note, both the superior and inferior mesenteric lymph nodes (sMLNs and iMLNs, respectively) were among the tissues that contained the highest titers of vRNA in animals on cART. Statistical analysis of vRNA in the lymphatic tissues also revealed significant suppression in group A as compared to controls (iliac and submandibular lymph nodes and iMLNs, $P=0.03$).

To identify the cell type(s) that support vRNA synthesis and, potentially, allow viral proteins to be produced during ART, we prepared tissue sections from the animals in group A and subjected them to *in situ* hybridization (ISH) and immunohistochemistry (IHC). While these tissues yielded no positive signals, the same staining techniques detected vRNA-positive cells and viral-protein-positive cells in tissue sections prepared from untreated animals (data not shown).

In summary, our initial questions were resolved as follows: the presence of vRNA in the gut, lungs, vagina, and lymphoid tissues indicated active viral replication in animals that were treated with cART for 1 year, and the lymphatic tissues allowed preferential viral replication in these animals.

SIV Nef-producing T lymphocytes predominated in the follicles of the MLNs from an animal that exhibited rebound of plasma viremia upon cessation of cART

Quantitative PCR analysis of vRNA in a variety of tissues collected from SIV-infected animals that were on prolonged chemotherapy (i.e., the animals in group A) indicated that the lymphatic tissues acted as the anatomic compartment for active virus replication during antiretroviral therapy. However, we were unable to identify histochemically any vRNA-positive or viral-protein-positive cells in the tissue sections prepared from these animals. This discrepancy was likely due to the lower sensitivity of these staining techniques as compared to PCR. We assumed that cessation of ART would result in rebound of plasma viremia, thereby promoting the transcription and translation of viral genes to levels detectable by the histochemical staining techniques employed in the present study. Based on this assumption, we took advantage of the rebound of plasma viremia as a surrogate approach to identify the viral reservoir(s) during cART. Thus, two Rhesus macaques (MM508 and MM511, designated as group B animals) were inoculated with the same SIV239 virus stock as was used to inoculate the group A animals. The group B animals exhibited an initial peak of viremia at 2 weeks pi (range, 7.7–8.4×10^7 copies/ml; Table 6), and the viral loads decreased and stabilized from 8 wpi onwards. Upon initiation of cART at 38 wpi, the levels of virus decreased rapidly and eventually fell below the limit of detection. The suppressed viral burdens were maintained until cessation of the treatment at 46 weeks pi. We attempted to determine the time-point at which the levels of viral gene transcription and translation were just above the detection limit of our staining. Since we envisioned that rebound of plasma viremia would take place within 2 weeks of interruption of therapy, animals were euthanized for necropsy on Day 10 after cessation of cART. The viral load in the plasma of animal MM511 was 1400 copies/ml, while that of animal

Table 6
Viral loads in plasma samples of animals in group B.

Animal ID	Plasma viral loads (copies/ml)					
	0 wpi	2 wpi	8 wpi	38 wpi	46 wpi	At autopsy[a]
MM508	<200	8.4×10^6	2.6×10^5	3.8×10^4	<200	<200
MM511	<200	7.7×10^6	3.1×10^5	1.1×10^5	<200	1.4×10^3

The animals were treated with cART from 38 wpi to 46 wpi.
[a] 47.5 wpi.

Table 7
Viral RNA burdens in various tissues collected from animals in group B.

Tissues	vRNA levels (copies/μg total RNA)	
	MM508 PVL, <200 copies/ml	MM511 PVL, 1400 copies/ml
Non-lymphoid tissues		
Heart	< 2900	< 2900
Liver	< 2900	< 2900
Kidney	< 2900	< 2900
CNS tissues		
Cerebrum	< 2900	< 2900
Cerebellum	< 2900	< 2900
Brain stem	< 2900	< 2900
Effector sites		
Lung	< 2900	< 2900
Vagina	< 2900	N.D.
Upper intestinal tract	< 2900	< 2900
Lower intestinal tract	< 2900	< 2900
Lymphoid tissues		
Spleen	**2.0×10^5**	**7.4×10^5**
Thymus	<2900	<2900
Iliac LN	**1.4×10^4**	**3.5×10^5**
Inguinal LN	<2900	**5.3×10^5**
Axillary LN	**1.9×10^4**	**1.3×10^6**
iMLN	**1.3×10^5**	**1.6×10^6**
sMLN	**8.4×10^3**	**1.5×10^6**
submandibular LN	**1.1×10^5**	**9.4×10^5**
Bronchial LN	**1.1×10^4**	**9.5×10^5**
Splenic LN	**9.9×10^4**	N.D.

PVL, plasma virus load; N.D., no data; CNS, central nervous system; LNs, lymph nodes; iMLNs, inferior mesenteric lymph nodes; sMLNs, superior mesenteric lymph nodes. Viral RNA (vRNA) levels greater than detection limit (2900 copies/μg total RNA) are represented in bold. vRNA levels are colored in grayscale as follows: white boxes, <2900; light-gray boxes, $<1.0 \times 10^5$; dark-gray boxes, $<1.0 \times 10^7$.

MM508 was below the limit of detection (Table 6). Thus, one animal was exhibiting rebound of plasma viremia while the other animal had not yet reached that stage when they were killed for analysis.

The overall tendency of the vRNA distribution in the group B animals was similar to that observed in the group A animals, with the titers being somewhat higher in group B. Higher levels of vRNA ($>1.0 \times 10^4$ copies/μg total RNA) were detected exclusively in the lymphoid tissues (Table 7). In MM511, the highest level of vRNA was detected in the MLNs ($>1.0 \times 10^6$ copies/μg total RNA). MM508, in which the plasma viral load was below the limit of detection at euthanasia, contained high levels of vRNA ($>1.0 \times 10^5$ copies/μg of total RNA), but only in the spleen and iMLN.

Based on the increased levels of vRNA transcription, we hypothesized that higher levels of viral proteins were synthesized in these two animals (MM508 and MM511) than in the group A animals. We subjected all the lymphoid tissues collected from these two animals to IHC, to identify viral-protein-producing cells. First, we focused on MM511, which exhibited higher viral titers in the plasma and lymphoid tissues than MM508, and stained tissue sections from this animal with anti-Nef antibodies. IHC yielded Nef-positive cells (Fig. 2). The viral-protein-positive cells were mainly localized to the globular architecture in the lymph node cortex, most likely the lymphoid follicles, and the Nef-positive cells bore morphologic characteristics similar to those of T lymphocytes (Fig. 2a). To clarify the architecture within which the Nef-producing cells were detected, we conducted combined IHC with an anti-Nef antibody (visualized with DAB) and an antibody directed against CD35 (visualized with VECTOR Blue). CD35 is a cell surface marker for FDCs, which are found exclusively in the follicles of the secondary lymphoid tissues. The combined staining showed that Nef-positive cells and FDCs were present in the same globular architecture, suggesting that the viral-protein-producing cells were predominantly located in the follicles of the lymph nodes of this animal. Moreover, staining revealed that the Nef-producing cells were juxtaposed on the FDCs (Fig. 2b).

To confirm the identity of the viral-protein-expressing cells, we conducted combined immunofluorescence staining with an anti-Nef antibody (visualized with Alexa Fluor 488) and an anti-CD3 antibody (visualized with Alexa Fluor 594). After extensive observations of the stained sections under the microscope, we detected Nef-positive cells in 16/305 sections prepared from a variety of lymphatic tissues collected from animal MM511, and these viral-protein-expressing cells were all positive for CD3 (Fig. 3 and Table 8). Of these 16 sections, 12 were prepared from MLNs and 4 from other anatomical

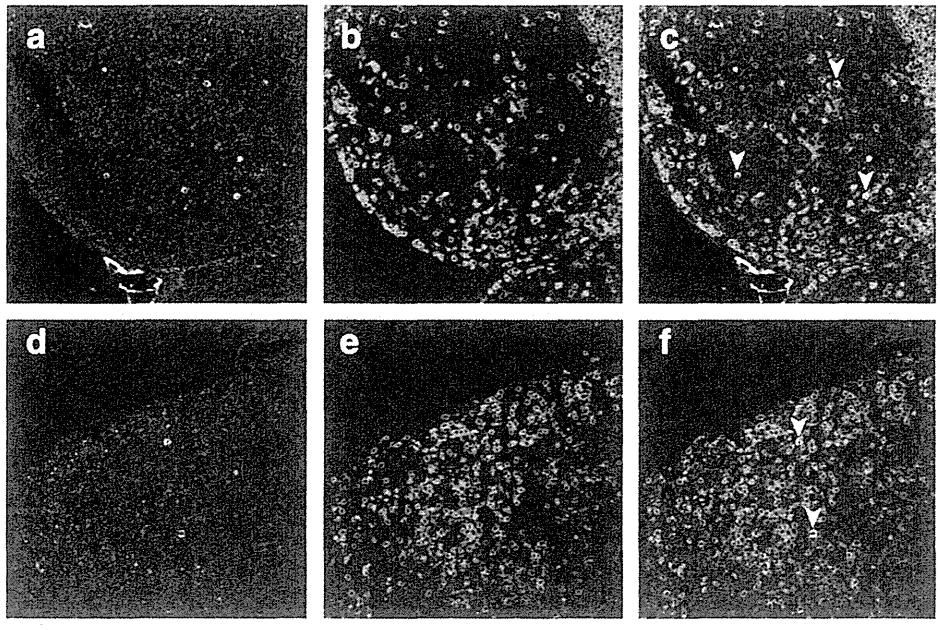

Fig. 3. Nef-positive T lymphocytes in the MLN of animal MM511. Tissue sections were stained using the anti-SIV Nef mouse monoclonal antibody (green, a and d) and the anti-CD3 rabbit polyclonal antibody (red, b and e). (c) Superimposed image of a and b. Nef-positive T cells are clustered in the follicles of the iMLN. (f) Superimposed image of d and e. The T cell is detected in the paracortical area of the sMLN. Original magnification, ×40.

compartments. The viral-protein-producing cells in the follicles constituted around 75% of all the positive cells detected. In some sections, Nef-positive cells were clustered in the follicles (Fig. 3c).

In animal MM508, which was subjected to analysis before rebound of plasma viremia had taken place, the staining revealed a single Nef-positive cell that was also positive for CD3 (data not shown). The frequency of positive cells in this animal was substantially lower (one positive cell in 136 sections) than that in MM511.

In summary, in the animal that exhibited rebound of plasma viremia after cessation of cART, almost all the viral-protein-synthesizing cells, presumably productively infected cells, that were detected in the MLNs were identified as T lymphocytes, most likely $CD4^+$ T cells. The vast majority of the virus-infected T cells were observed in the lymphoid follicles during rebound of plasma viremia (Table 8).

Discussion

The presence in infected individuals of HIV-1 viral reservoirs that persist during HAART impedes curing and complete eradication of the virus. While studies have been conducted into the identity and properties of the HIV-1 reservoirs (Brennan et al., 2009; Chun et al., 2000; Sharkey et al., 2011), much remains to be learnt. We reasoned that systemic analyses of infected individuals who were undergoing intensive ART would advance the characterization of the viral reservoirs (Dinoso et al., 2009; North et al., 2009). Therefore, we analyzed SIV-infected Rhesus macaques that underwent cART for 1 year. The major finding of the current study is that lymphatic tissues, including MLNs, contained higher numbers of cellular virus reservoirs that potentially cause rebound of plasma viremia upon cessation of cART. This assertion is based on the following observations: the lymphatic tissues contained the highest levels of vRNA in all the animals, regardless of cART, and the viral-protein-expressing T cells were localized predominantly to the MLNs of the animal that exhibited rebound of plasma viremia after cessation of cART.

We finalized the drug dosages to be administered by monitoring plasma trough levels of antiviral activity at 14 h post-consumption. During this process we discovered that the drug metabolism of monkeys is somewhat higher than that of humans. To fine-tune the drug concentrations in the circulation, 50% of the dosage established in the present study, corresponding to 150% of the dosage for a 60-kg adult patient, was given to the same animals. The circulating drug concentration at 14 h post-consumption yielded no measurable net antiviral activity (data not shown). Therefore, it is necessary to determine an appropriate dosage for each drug prior to administration to animals. In this regard, one of the monkeys in group A, MM499, exhibited fluctuating antiviral activity during the therapy. At 10 and 64 weeks pi, the antiviral activity in the blood was below the recommended trough level for patients (1.5 μM) (Table 4). Despite the fluctuation of antiviral activity, the viral burden of this animal was maintained below the limit of detection during the therapy, and systemic analysis revealed levels of vRNA that were comparable to those detected in the other three animals in group A (Table 5). That the other three animals also exhibited fluctuating concentrations of the drug in the circulation underlines the importance of monitoring antiviral activity in circulation during therapy, to ensure that the administration schedule produces the expected antiviral activity.

RT-PCR analyses revealed that lymphatic tissues contained higher titers of vRNA than the other tissues in 4/4 SIV-infected macaques in group A, and 2/2 animals in group B followed the same distribution of vRNA (Tables 5 and 7). In SIV-infected monkeys treated with cART, the Lamivudine concentration was more than 300-fold higher in the gastrointestinal tract than in the peripheral lymph nodes (Bourry et al., 2010). The finding of Bourry et al. explains our observation that chemotherapy was more effective at suppressing virus replication in the intestine than in the lymph nodes. It is possible that lymphatic tissues serve as viral sanctuaries, especially when the amount of drug accumulated in the tissues is insufficient to suppress virus replication. It should be noted that while viral load and drug concentration in the plasma are easily monitored, they do not reflect precisely the virus replication/drug distribution in specific important anatomic compartments.

Our results are also in good agreement with the results reported by North et al., who performed a thorough analysis of a variety of tissues collected from RT-SHIV-infected animals that were receiving combined anti-viral therapy (North et al., 2009). The authors employed RT-SHIV, which is a chimeric virus that carries the HIV-1-derived RT gene on the backbone of SIV239, to model HAART to patients, in the context of SIV, since non-nucleotide reverse-transcriptase inhibitors (NNRTIs), one of the core components of HAART, do not suppress reverse transcription mediated by SIV RT (Balzarini et al., 1995). Although the cART regimen devised in the current study is unlike the HAART administered to patients, especially with respect to the employment of certain drugs, the viral decay rate in the circulation (calculated based on a two-compartment model) is comparable to that observed in patients treated with the multi-drug regimen (Murray et al., 2007; Palmer et al., 2008; Perelson et al., 1997) (Table 2 and Supplemental Fig. 2). Therefore, it is implied that the lymphatic tissues may harbor higher titers of vRNA in HIV-1-infected patients on HAART, despite the viral burdens in the circulation are clinically non-detectable. The caveat is that the animals in the current study were on treatment for up to 1 year only, which is a considerably shorter treatment period than that of patients who have achieved successful virus containment since the beginning of the HAART era. Given that the desired concentration of the drug may not be reached in the lymphatic tissues, it is necessary to devise a way to deliver in a preferential manner either antiviral drugs or a specific injury to these compartments, in combination of HAART, to achieve eradication of the virus, which is a crucial step toward a complete cure for HIV-1 infection.

Histochemical analyses revealed that the SIV Nef protein was expressed in T lymphocytes predominantly resident in the follicles formed in the MLNs of animal MM511, which exhibited viral rebound after cessation of cART (Fig. 3 and Table 8). Active virus replication in the follicles of lymph nodes has been described (Folkvord et al., 2005). Previous studies have suggested that lymphatic follicles serve as preferred sites of virus replication, probably *via* FDCs and sequestration of virus-infected cells from cytotoxic T lymphocytes (CTLs). FDCs, which may interact with $CD4^+$ cells within the "enclave", retain infectious virus particles and produce TNF-α, which promotes HIV replication (Thacker et al., 2009). HIV-1-specific CTLs fail to accumulate within lymphoid follicles, allowing unchecked virus replication in this architecture (Connick et al., 2007). Taken together, these findings support our observations of active viral protein synthesis in the lymphoid follicles.

The present study does not identify definitively the viral reservoirs. However, it does not rule out any of the proposed candidate reservoirs: resting $CD4^+$ T lymphocytes, FDCs, and unidentified cells involved in ongoing virus replication during therapy. To place our results in the context of current thinking regarding putative viral reservoirs, we make the following important points:

Table 8
Numbers of immunohistochemistry sections examined from macaques in group B.

Nef expressing T cells	Number of sections subjected				
	MM508		MM511		
	MLN	Non-MLN	MLN	Non-MLN	Total
Present in the follicles	0	0	9	3	12
Present in the paracortical area	1	0	3	1	5
Absent	50	85	34	255	424

MLNs; mesenteric lymph nodes.

North et al.(2009) detected proviral DNA in the resting $CD4^+$ T-lymphocyte fraction prepared from MLNs. Dinoso et al.(2009) recovered replication-competent viruses in the cell fraction. It is possible that the Nef-positive cells detected in the current study were reactivated upon stimulation, thereby prompting resumption of the virus replication cycle; the progeny viral particles from these cells would initiate multiple rounds of replication in the T cells of the paracortical area and the follicles of the lymph nodes.

We detected FDCs juxtaposed on the Nef protein-positive T lymphocytes. This observation is not definitive evidence that FDCs transmit infectious viral particles to $CD4^+$ T cells. Based on our observations, we hypothesize that FDCs transmit virus to $CD4^+$ T cells or stimulate infected cells, so as to initiate viral rebound. An important caveat is that the animal in question was treated for only 8 weeks. Since FDCs are known to retain virus particles with their infectivity intact for a certain period of time (Keele et al., 2008), it would be informative to determine whether the interaction between these two cell types occurs in animals that exhibit rebound after a prolonged period of therapy, followed by cessation.

Although we have no direct evidence that unknown cells are involved in ongoing viral replication during therapy, higher titers of vRNA were detected in the lymphatic tissues, primarily the MLNs, which suggests that certain cell types in this compartment allow viral replication during chemotherapy. It is likely that the levels of transcription of viral genes and of subsequent translation are too low to be detected by the staining techniques employed in the current study.

Based on our results, we postulate the following sequence of events after the cessation of HAART in individuals infected with HIV-1: in the follicles of the lymph nodes, such as MLNs, viruses that are preserved in certain forms, such as intact genomes and infectious particles, and with low-level ongoing replication, resume a productive replication cycle, preceding other anatomical compartments, when the concentration of the antiviral drug declines due to discontinuation of therapy; thereafter, other anatomic compartments resume productive viral replication owing to weakened containment of the virus and higher accumulations of the drugs. The progeny viral particles produced from the tissues subsequently enter the circulation and cause rebound of plasma viremia, i.e., systemic viral replication.

Considering that the state-of-the-art histochemical staining still has lower sensitivity than PCR and that the vRNA distributions for animals on ART and those with rebound of plasma viremia are similar, analyses of animals undergoing rebound of plasma viremia after discontinuation of therapy could serve as a surrogate approach to study virus reservoirs during HAART.

Fortunately, we captured ongoing rebound of plasma viremia in animal MM511, whose viral burden was above the detection limit defined by the current staining technique. Further fine-tuning in the duration of therapy and timing of analysis after cessation would provide better clues to the identity of virus reservoirs.

Materials and methods

Cells

Human embryonic kidney-derived 293T cells were cultured in Dulbecco's modified Eagle's medium (D-MEM; Invitrogen, Carlsbad, CA) that was supplemented with 10% fetal bovine serum (FBS; HyClone Laboratories, Logan, UT) and 2 mM L-glutamine. Human T-lymphoid MT-4 (Harada et al., 1985), Molt-4 (Koyanagi et al., 1986), and M8166 (Shibata et al., 1991) cells were cultured in RPMI 1640 medium (Invitrogen) that was supplemented with 10% FBS, 2 mM sodium pyruvate, and 4 mM L-glutamine (R-10). Rhesus macaque PBMCs were prepared from whole blood that was anticoagulated with EDTA in lymphocyte separation medium (Nakalai Tesque, Kyoto, Japan). PBMCs were resuspended in R-10 medium that was supplemented with 40 μg/ml gentamicin, 50 μM 2-mercaptoethanol, and 25 μg/ml concanavalin A (Sigma-Aldrich, St. Louis, MO), and cultured for 16–20 h at 37 °C. Before virus infection, the cells were cultured for an additional 2 days in R-10 medium that was supplemented with 40 μg/ml gentamicin, 50 μM 2-mercaptoethanol, and 100 IU/ml recombinant human IL-2 (Imunace; Shionogi, Osaka, Japan).

Viruses

The stock of SIV239 used in the tissue culture and animal experiments was prepared in Rhesus macaque PBMCs inoculated with the supernatant of a 293T-cell culture that was transiently transfected with full-length infectious molecular clones of the virus (Kestler et al., 1990). A stock of HIV-1 IIIB (Popovic et al., 1984) was prepared from the supernatant of a Molt-4 cell culture that was chronically infected with the virus. The SIV239 stock was titrated by infection of M8166 cells, and the number of infectious units was calculated by a method described previously (Reed and Muench, 1938).

Animal experiments

Female Rhesus macaques of Chinese or Indian origin, 4 kg in body weight, were used for experimental infection with SIV239. Phlebotomy and virus inoculation were carried out under anesthesia by intramuscular injection of a mixture of ketamine chloride (Ketalar; Daiichi Sankyo, Tokyo, Japan) at 5–10 mg/kg and xylazine chloride (Celactal; Bayer Healthcare, Leverkusen, Germany) at 1.5–2.0 mg/kg. For virus infection, animals were inoculated intravenously with 2000-times the 50% tissue culture infectious doses ($TCID_{50}$) of SIV239. Animal experiments were conducted in a biosafety level 3 animal facility, in compliance with institutional regulations approved by the Committee for Experimental Use of Nonhuman Primates of the Institute for Virus Research, Kyoto University, Kyoto, Japan.

Extraction of active components from drug tablets or plasma

Saquinavir (Invirase; Chugai Pharmaceutical, Tokyo, Japan), Lopinavir/Ritonavir (Kaletra; Abbott Laboratories, Abbott Park, IL), and Atazanavir (Reyataz; Bristol-Myers Squibb, New York, NY) were purchased from their respective sources. Drug tablets were pulverized with a pestle and mortar and dissolved in dimethyl sulfoxide (DMSO; Wako Pure Chemical Industries, Osaka, Japan). The concentration of each drug in DMSO was adjusted to 100 μg/ml with RPMI 1640 medium. To simulate the conditions of the drugs in the blood, the drug solutions were diluted 10-fold with normal plasma from Rhesus macaque. The drug extract was subsequently deproteinized by mixing with methanol/acetonitrile (1:1). The soluble fraction was evaporated, subsequently reconstituted in RPMI 1640 medium, and adjusted to a concentration of 20 μg/ml. Plasma samples collected from the animals were deproteinized, evaporated, and reconstituted as described above. The efficacy of the extraction employed in the current study ranged from 30 to 50% when assessed using the anti-HIV-1 drugs AZT, SQV, and RTV (data not shown).

Virus inhibition assay (MT-4/MTT assay)

The efficacies of the PIs against SIV were assessed as described previously (Sato et al., 1995), with minor modifications. Briefly, aliquots of 5×10^3 MT-4 cells were dispensed into 96-well round-bottomed tissue culture plates. Serially diluted extracts of the HIV-1 PIs or extracts of animal plasma samples were incubated with the cells in quadruplicate at 37 °C for 1 h. The cells were then inoculated with 1.8×10^3 $TCID_{50}$ of SIV239 or 0.9×10^2 $TCID_{50}$ of HIV-1 IIIB (multiplicity of infection [MOI] = 0.37 or 0.018, respectively). On Day 5

pi, the viability of the cells was assessed by adding the MTT reagent (Nakalai Tesque).

Formulation and feeding of drugs and diet

The daily dosages of the drugs were half of those recommended for an adult human, i.e., 300 mg of AZT and 150 mg of 3TC (as Combivir; GlaxoSmithKline, London, UK), 150 mg of Tenofovir disproxil fumarate (TDF, as Viread; Japan Tobacco, Tokyo, Japan), and 400 mg of Lopinavir and 100 mg of Ritonavir (as Kaletra; Abbott). To correlate these dosages for a 4-kg Rhesus macaque with the recommended dosage for an adult human, the body surface area (BSA) of the monkeys was computed as described previously (Du Bois and Du Bois, 1915, 1916). Using BSA and body weight, the *Km* factor for each animal was derived as described (Reagan-Shaw et al., 2008). The dosage for the monkeys corresponded to 3-fold that for an adult human weighing 60 kg. Among the drugs selected, Combivir (AZT/3TC) and Kaletra (LPV/RTV) should be taken twice a day to maintain effective drug concentrations. Therefore, two sets of drug/diet were prepared. Formulation #1 contained AZT, 3TC, LPV, and RTV (150 mg, 75 mg, 200 mg, and 50 mg, respectively), while formulation #2 contained all the drugs in formulation #1 plus TDF (150 mg). Thirty-five grams of primate diet for Old World monkeys (Lab Diet 5048; PMI Nutrition International, Henderson, CO), granulated with a bar blender, was combined with the pulverized drugs. The drug/diet mixture was further mixed with 75 g of squashed banana and formed into a rectangular plate. The formulated drug/diet described above was given to animals in place of their normal diet. Drug/diet formulation #1 was given in the morning and formulation #2 was given 10 h later, at intervals of 10 h and 14 h per day. Seven of the nine Rhesus macaques that were fed the formulated drug/diet ingested 80–90% of total mass within 2 h.

To assess the potential adverse effects of the high-dosage drug administration employed in the current study, serum samples collected from these animals before and during cART were submitted to analyses for the following clinical markers: blood urea nitrogen (BUN), creatinine, total cholesterol, and triglycerides. No substantial fluctuations were observed before and during cART in the values for BUN (average values: for MM491, 16.8 mg/dl; for MM499, 16.0 mg/dl; for MM528, 16.7 mg/dl; and for MM530, 20.9 mg/dl), creatinine (average values: for MM491, 0.5 mg/dl; for MM499, 0.6 mg/dl; for MM528, 0.5 mg/dl; and for MM530, 0.5 mg/dl), and total cholesterol (average values: for MM491, 153 mg/dl; for MM499, 106 mg/dl; for MM528, 109 mg/dl; and for MM530, 132 mg/dl). Nearly all the samples analyzed fell within the normal value ranges for the above-mentioned markers (data not shown). The triglyceride values from all the treated animals, with the exception of MM499, increased upon onset of ART: for MM491, the values ranged from 28 mg/dl at pretreatment to 99 mg/dl at maximum during cART; for MM528, from 21 mg/dl to 58 mg/dl; and for MM530, from 48 mg/dl to 129 mg/dl. The published normal value range for triglycerides in Rhesus macaques is 24–42 mg/dl (Fortman et al., 2001). At autopsy, lipid deposition in the liver was noted in MM530, which exhibited the highest mean level of triglycerides among the three animals, indicative of a certain degree of dysregulation of lipid metabolism. Despite the increase in triglyceride levels, all the treated animals were clinically healthy.

Lopinavir measurement by high-performance liquid chromatography

The drug concentrations in the blood samples were measured by high-performance liquid chromatography (HPLC) as described previously (Frappier et al., 1998), with minor modifications. Briefly, plasma samples collected from two monkeys were subjected to deproteinization by the addition of acetonitrile, and were subsequently loaded onto a HPLC column. The assay conditions were as follows: column, ODS column (150 mm in length and 4.6 mm in diameter; Cadenza); mobile phase, gradient prepared from two solutions (solution A, 0.1% trifluoroacetic acid [TFA] in water; solution B, 0.1% TFA in acetonitrile). The total flow rate was 0.6 ml/min. For detection of the compound, UV absorbance at a wavelength of 215 nm was employed.

Plasma viral RNA measurement

Viral RNA loads in plasma were measured as described previously (Miyake et al., 2006). Briefly, total RNA was extracted from plasma samples with the QIAamp Viral RNA kit (Qiagen, Valencia, CA). The extracted RNA samples were subjected to RT-PCR to amplify the SIV gag region using the TaqMan EZ RT-PCR kit (PerkinElmer, Wellesley, MA). The PCR and detection of products were performed in a Prism 7700 Sequence Detector (Applied Biosystems, Foster City, CA). The primer pair employed for PCR amplification was SIV2-696F (5′-GGAAATTACCCAGTACAACAAA-TAFF-3′) and SIV2-784R (5′-TCTATCAATTTTACCCAggCATTTA-3′). PCR products were detected with a labeled probe, SIV2-731T (5′-Fam-TGTCCACCTGCCATTAAGCCCG-Tamra-3′; Perkin Elmer).

Selected plasma samples from monkeys on cART (at 29, 42, and 52 weeks pi, and at euthanasia) were further subjected to quantitative real-time PCR with a lower detection limit, following the method described by Cline et al., with modifications (Cline et al., 2005). Briefly, 1.5-ml plasma samples were centrifuged at 20,000×*g* for 1 h to sediment virus particles. The pellets were incubated with a mixture of GuHCl (Sigma-Aldrich) and proteinase K (Invitrogen) for 60 min at 37 °C and subsequently incubated with a mixture of GuSCN (Sigma-Aldrich) and glycogen (Roche Applied Science, Indianapolis, IN) for 5 min at room temperature, followed by precipitation with isopropanol. The precipitated RNA fractions were resuspended in water and subjected to RT-PCR, as described above. A standard curve of the reaction was constructed by plotting threshold cycles of serially diluted virus stocks containing known amounts of vRNA extracted in the same manner as the test plasma samples. The detection limit was defined by the standard curve with a correlation coefficient (>0.96) constructed from a set of serial dilutions with reproducible amplification. The detection limit of the assay was consistently <20 copies/ml.

Mathematical modeling and statistical analysis of decay rate

The decline in SIV239 RNA copies in the plasma during cART was evaluated using a mathematical model similar to that developed previously to quantify and analyze the decay of HIV-1 viremia in patients treated with combination anti-retroviral therapy (Perelson et al., 1997). Briefly, two distinct cellular compartments are assumed to contribute to the vRNA. The first compartment consists of $CD4^+$ T cells (i.e., short-lived cells), *T*, which are infected with a constant, *k*, die with a rate constant, δ, and have a burst size of *N*. The second compartment consists of long-lived cells, *M*, which become infected with a rate constant, k_M, die with a rate, μ_M, and produce p virions per cell. Free virus particles are cleared with a constant, c. Assuming that viral inhibition by cART is 100%, *de novo* infection is completely blocked in this mathematical model. Then, using the parameters explained above, the overall vRNA copies in the plasma can be described by the following equation:

$$V(t) = V_0\left\{\left(1-\frac{NkT_0}{c-\delta}-\frac{c-NkT_0}{c-\mu_M}\right)e^{-ct}+\frac{NkT_0}{c-\delta}e^{\delta t}+\frac{c-NkT_0}{c-\mu_M}e^{\mu M t}\right\}. \quad (1)$$

Here, V_0 and T_0 are the steady-state level of viral load and $CD4^+$ T cells count before HAART, respectively. The derivation of Eq. (1) is explained in detail elsewhere (Perelson and Nelson, 1999). To fit the plasma viremia data with the two-compartment model, we estimated the parameters, δ, μ_M, and a composite parameter, NkT_0, employing

nonlinear least-squares regression (FindMinimum package of Mathematica ver. 7.0 software). Since virion clearance occurs too rapidly to estimate c from the available data in Rhesus macaques, we fixed $c=62.1$ (determined previously) (Igarashi et al., 1999), although the change in c did not significantly change in our parameter estimates (data not shown). To derive the 68% confidence interval for each parameter, we employed a bootstrap method (Efron, 1979; Efron and Tibshirani, 1986) in which each experiment was simulated 1000 times. Statistical comparisons for continuously distributed variables between groups were performed with Welch's test. Nominal P-values <0.05 were considered statistically significant and all tests were two-sided.

Necropsy and tissue collection

All the animals were subjected to perfusion/euthanasia, as described previously (Igarashi et al., 2002), with minor modifications. Briefly, animals anesthetized with ketamine/xylazine were intravenously administered pentobarbital sodium (50 mg/kg body weight, Nembutal; Abbott Laboratories) before thoracotomy. The right atrium was incised and one liter of sterile saline anti-coagulated with heparin (5 U/ml) was introduced into the left ventricle *via* a 16G needle attached to infusion tubing. Peripheral blood was collected prior to perfusion. During the perfusion, tissue collection was conducted. Collected tissues were trimmed and placed into two independent workflows: submersion in RNA*later* (Qiagen) and stored at −20 °C until RNA extraction, and fixation in 4% paraformaldehyde in PBS at 4 °C overnight, followed by embedding in paraffin wax for histopathologic analyses. The list of collected tissues is summarized in Table 5.

Isolation, quantification, and statistical analysis of viral RNA from tissues

Tissues submerged in RNA*later* and stored at −20 °C were subjected to total RNA extraction using TRIzol reagent (Invitrogen) according to the manufacturer's recommendations. Briefly, 50–100 mg of each tissue resuspended in 1 ml of TRIzol reagent were homogenized with Lysing Matrix D (MP Biomedicals, Irvine, CA) using FastPrep FP120 (MP Biomedicals). Chloroform (0.2 ml) was added to the homogenate, and the aqueous phase was collected to a new tube after centrifugation at 12,000×g for 15 min at 4 °C. The aqueous phase was mixed with 0.5 ml isopropanol, and the supernatant was removed after centrifugation at 12,000×g for 10 min at 4 °C. Then, 1 ml of 75% ethanol was added to the pellet and, after centrifugation at 7500×g for 5 min at 4 °C, the supernatant was cleared. The total RNA sample was resuspended in RNase-free water and frozen at −80 °C until use. The amount of RNA extracted from each tissue specimen was measured in a UV spectrophotometer (UV-1600; Shimadzu, Kyoto, Japan). Aliquots (1 μg) of RNA extracted from the various tissue samples were subjected to RT-PCR, to amplify the SIV gag region. The amounts of vRNA detected by PCR in a variety of tissues from treated animals and untreated controls, as described below, were compared using a Mann–Whitney test and GraphPad Prism software (GraphPad, La Jolla, CA).

Immunohistochemistry

Viral-protein-producing cells were visualized with an anti-SIV antibody and anti-CD35 antibody, as described previously (Inaba et al., 2009), with minor modifications. Briefly, tissue sections (4-μm thickness) were dewaxed with xylene, rehydrated through an alcohol gradient, submerged in Target Retrieval Solution (DAKO, Glostrup, Denmark), and processed in an autoclave for 10 min to unmask the antigens. Subsequently, the tissue sections were washed with Tris-buffered saline/Tween-20 (TBST), treated with REAL Peroxidase-Blocking Solution (DAKO) for 5 min, to deactivate endogenous peroxidase, and washed with TBST. The sections were incubated with an anti-SIV Nef mouse monoclonal antibody (diluted 1:500, clone 04-001; FIT Biotech, Tampere, Finland) at 4 °C overnight. After washing with TBST, the sections were incubated at room temperature for 30 min with the Envision+ kit (a horseradish peroxidase-labeled anti-mouse immunoglobulin polymer; DAKO), washed with TBST, visualized using diaminobenzidine (DAB) substrate (DAKO) as the chromogen, and rinsed in distilled water. Subsequently, the sections were treated at 95 °C for 10 min with Target Retrieval Solution (DAKO), to deactivate the antibody added upstream in the procedure, washed with TBST, and incubated with the anti-CD35 mouse monoclonal antibody (diluted 1:50, clone Ber-MAC-DRC; DAKO) at 4 °C overnight. After washing, the slides were incubated with Histofine Simple Stain AP (an alkaline phosphatase-labeled anti-mouse immunoglobulin polymer; Nichirei, Tokyo, Japan) at room temperature for 30 min, and washed with TBST. The specific antigen-antibody reaction was visualized with Blue Alkaline Phosphatase Substrate Kit III (Vector Laboratories, Burlingame, CA). The stained sections were examined under an Axiophot Universal microscope (Carl Zeiss, Oberkochen, Germany), and images were captured with the Nikon Digital Sight DS-Fi1 camera head and Nikon Digital Sight DS-L2 control unit (Nikon, Tokyo, Japan).

To identity the Nef-producing cells, slides of the tissue were stained with the anti-SIV antibody and anti-CD3 antibody. Sections were subjected to dewaxing and unmasking of antigens, as described above. Subsequently, the sections were incubated with the anti-SIV Nef mouse monoclonal antibody (diluted 1:500, clone 04-001; FIT Biotech) at 4 °C overnight. After washing with TBST, the sections were incubated at room temperature for 30 min with anti-CD3 rabbit polyclonal antibody (diluted 1:50; DAKO), and washed with TBST. The sections were treated with Alexa Fluor 488 (diluted 1:200, fluorochrome-conjugated goat anti-mouse immunoglobulin G; Molecular Probes, Eugene, OR) and Alexa Fluor 594 (diluted 1:200; fluorochrome-conjugated goat anti-rabbit immunoglobulin G; Molecular Probes) for 1 h, to visualize the bound anti-SIV Nef antibody and anti-CD3 antibody, respectively. The stained sections were examined using a Leica TCS SP2 AOBS confocal microscope (Leica Microsystems, Exton, PA) and the Leica image software (Leica Microsystems). Sections prepared from an SIV-infected monkey (MM521) and uninfected monkeys were stained in the same manner as those from cART and post-cART animals, as controls for the staining (Supplemental Fig. 3).

Supplementary materials related to this article can be found online at doi:10.1016/j.virol.2011.11.024.

Acknowledgment

The authors are in debt to Drs. T. Sata and S. Nakamura for technical advice and critique on histochemical staining, Dr. A. Nomoto for continuous support, and member of the Igarashi laboratory for assistance of animal procedures and analyses. This work was supported by Research on HIV/AIDS [08062160 to T.I.] from the Ministry of Health, Labor and Welfare of Japan. S.I. was supported by JST PRESTO program.

References

Balzarini, J., Weeger, M., Camarasa, M.J., De Clercq, E., Uberla, K., 1995. Sensitivity/resistance profile of a simian immunodeficiency virus containing the reverse transcriptase gene of human immunodeficiency virus type 1 (HIV-1) toward the HIV-1-specific non-nucleoside reverse transcriptase inhibitors. Biochem. Biophys. Res. Commun. 211 (3), 850–856.

Benlhassan-Chahour, K., Penit, C., Dioszeghy, V., Vasseur, F., Janvier, G., Riviere, Y., Dereuddre-Bosquet, N., Dormont, D., Le Grand, R., Vaslin, B., 2003. Kinetics of lymphocyte proliferation during primary immune response in macaques infected with pathogenic simian immunodeficiency virus SIVmac251: preliminary report of the effect of early antiviral therapy. J. Virol. 77 (23), 12479–12493.

Bourry, O., Mannioui, A., Sellier, P., Roucairol, C., Durand-Gasselin, L., Dereuddre-Bosquet, N., Benech, H., Roques, P., Le Grand, R., 2010. Effect of a short-term HAART on SIV load in macaque tissues is dependent on time of initiation and antiviral diffusion. Retrovirology 7, 78.

Brenchley, J.M., Schacker, T.W., Ruff, L.E., Price, D.A., Taylor, J.H., Beilman, G.J., Nguyen, P.L., Khoruts, A., Larson, M., Haase, A.T., Douek, D.C., 2004. CD4+ T cell depletion

during all stages of HIV disease occurs predominantly in the gastrointestinal tract. J. Exp. Med. 200 (6), 749–759.
Brennan, T.P., Woods, J.O., Sedaghat, A.R., Siliciano, J.D., Siliciano, R.F., Wilke, C.O., 2009. Analysis of human immunodeficiency virus type 1 viremia and provirus in resting CD4+ T cells reveals a novel source of residual viremia in patients on antiretroviral therapy. J. Virol. 83 (17), 8470–8481.
Burton, G.F., Keele, B.F., Estes, J.D., Thacker, T.C., Gartner, S., 2002. Follicular dendritic cell contributions to HIV pathogenesis. Semin. Immunol. 14 (4), 275–284.
Buzon, M.J., Massanella, M., Llibre, J.M., Esteve, A., Dahl, V., Puertas, M.C., Gatell, J.M., Domingo, P., Paredes, R., Sharkey, M., Palmer, S., Stevenson, M., Clotet, B., Blanco, J., Martinez-Picado, J., 2010. HIV-1 replication and immune dynamics are affected by raltegravir intensification of HAART-suppressed subjects. Nat. Med. 16 (4), 460–465.
Chun, T.W., Davey Jr., R.T., Engel, D., Lane, H.C., Fauci, A.S., 1999. Re-emergence of HIV after stopping therapy. Nature 401 (6756), 874–875.
Chun, T.W., Davey Jr., R.T., Ostrowski, M., Shawn Justement, J., Engel, D., Mullins, J.I., Fauci, A.S., 2000. Relationship between pre-existing viral reservoirs and the re-emergence of plasma viremia after discontinuation of highly active anti-retroviral therapy. Nat. Med. 6 (7), 757–761.
Chun, T.W., Stuyver, L., Mizell, S.B., Ehler, L.A., Mican, J.A., Baseler, M., Lloyd, A.L., Nowak, M.A., Fauci, A.S., 1997. Presence of an inducible HIV-1 latent reservoir during highly active antiretroviral therapy. Proc. Natl. Acad. Sci. U. S. A. 94 (24), 13193–13197.
Cline, A.N., Bess, J.W., Piatak Jr., M., Lifson, J.D., 2005. Highly sensitive SIV plasma viral load assay: practical considerations, realistic performance expectations, and application to reverse engineering of vaccines for AIDS. J. Med. Primatol. 34 (5–6), 303–312.
Connick, E., Mattila, T., Folkvord, J.M., Schlichtemeier, R., Meditz, A.L., Ray, M.G., McCarter, M.D., Mawhinney, S., Hage, A., White, C., Skinner, P.J., 2007. CTL fail to accumulate at sites of HIV-1 replication in lymphoid tissue. J. Immunol. 178 (11), 6975–6983.
Dinoso, J.B., Rabi, S.A., Blankson, J.N., Gama, L., Mankowski, J.L., Siliciano, R.F., Zink, M.C., Clements, J.E., 2009. A simian immunodeficiency virus-infected macaque model to study viral reservoirs that persist during highly active antiretroviral therapy. J. Virol. 83 (18), 9247–9257.
Douek, D.C., Picker, L.J., Koup, R.A., 2003. T cell dynamics in HIV-1 infection. Annu. Rev. Immunol. 21, 265–304.
Du Bois, D., Du Bois, E.F., 1915. The measurement of the surface area of man. Arch. Intern. Med. 15, 868–881.
Du Bois, D., Du Bois, E.F., 1916. A formula to estimate the approximate surface area if height and weight be known. Arch. Intern. Med. 17, 863–871.
Efron, B., 1979. 1977 Rietz lecture – bootstrap methods – another look at the Jackknife. Ann. Stat. 7 (1), 1–26.
Efron, B., Tibshirani, R., 1986. Bootstrap methods for standard errors, confidence intervals, and other measures of statistical accuracy. Stat. Sci. 1, 54–75.
Embretson, J., Zupancic, M., Ribas, J.L., Burke, A., Racz, P., Tenner-Racz, K., Haase, A.T., 1993. Massive covert infection of helper T lymphocytes and macrophages by HIV during the incubation period of AIDS. Nature 362 (6418), 359–362.
Finzi, D., Hermankova, M., Pierson, T., Carruth, L.M., Buck, C., Chaisson, R.E., Quinn, T.C., Chadwick, K., Margolick, J., Brookmeyer, R., Gallant, J., Markowitz, M., Ho, D.D., Richman, D.D., Siliciano, R.F., 1997. Identification of a reservoir for HIV-1 in patients on highly active antiretroviral therapy. Science 278 (5341), 1295–1300.
Folkvord, J.M., Armon, C., Connick, E., 2005. Lymphoid follicles are sites of heightened human immunodeficiency virus type 1 (HIV-1) replication and reduced antiretroviral effector mechanisms. AIDS Res. Hum. Retroviruses 21 (5), 363–370.
Fortman, J.D., Hewett, T.A., Bennett, B.T., 2001. The Laboratory Nonhuman Primate. CRC Press, New York.
Frappier, S., Breilh, D., Diarte, E., Ba, B., Ducint, D., Pellegrin, J.L., Saux, M.C., 1998. Simultaneous determination of ritonavir and saquinavir, two human immunodeficiency virus protease inhibitors, in human serum by high-performance liquid chromatography. J. Chromatogr. B Biomed. Sci. Appl. 714 (2), 384–389.
Frost, S.D., Gunthard, H.F., Wong, J.K., Havlir, D., Richman, D.D., Leigh Brown, A.J., 2001. Evidence for positive selection driving the evolution of HIV-1 env under potent antiviral therapy. Virology 284 (2), 250–258.
Giuffre, A.C., Higgins, J., Buckheit Jr., R.W., North, T.W., 2003. Susceptibilities of simian immunodeficiency virus to protease inhibitors. Antimicrob. Agents Chemother. 47 (5), 1756–1759.
Guadalupe, M., Reay, E., Sankaran, S., Prindiville, T., Flamm, J., McNeil, A., Dandekar, S., 2003. Severe CD4+ T-cell depletion in gut lymphoid tissue during primary human immunodeficiency virus type 1 infection and substantial delay in restoration following highly active antiretroviral therapy. J. Virol. 77 (21), 11708–11717.
Harada, S., Koyanagi, Y., Yamamoto, N., 1985. Infection of HTLV-III/LAV in HTLV-I-carrying cells MT-2 and MT-4 and application in a plaque assay. Science 229 (4713), 563–566.
Havlir, D.V., Strain, M.C., Clerici, M., Ignacio, C., Trabattoni, D., Ferrante, P., Wong, J.K., 2003. Productive infection maintains a dynamic steady state of residual viremia in human immunodeficiency virus type 1-infected persons treated with suppressive antiretroviral therapy for five years. J. Virol. 77 (20), 11212–11219.
Igarashi, T., Brown, C., Azadegan, A., Haigwood, N., Dimitrov, D., Martin, M.A., Shibata, R., 1999. Human immunodeficiency virus type 1 neutralizing antibodies accelerate clearance of cell-free virions from blood plasma. Nat. Med. 5 (2), 211–216.
Igarashi, T., Brown, C.R., Byrum, R.A., Nishimura, Y., Endo, Y., Plishka, R.J., Buckler, C., Buckler-White, A., Miller, G., Hirsch, V.M., Martin, M.A., 2002. Rapid and irreversible CD4+ T-cell depletion induced by the highly pathogenic simian/human immunodeficiency virus SHIV(DH12R) is systemic and synchronous. J. Virol. 76 (1), 379–391.
Inaba, K., Fukazawa, Y., Matsuda, K., Himeno, A., Matsuyama, M., Ibuki, K., Miura, Y., Koyanagi, Y., Nakajima, A., Blumberg, R.S., Takahashi, H., Hayami, M., Igarashi, T., Miura, T., 2009. Small intestine CD4+ cell reduction and enteropathy in simian/human immunodeficiency virus KS661-infected rhesus macaques in the presence of low viral load. J. Gen. Virol. 91 (Pt 3), 773–781.
Keele, B.F., Tazi, L., Gartner, S., Liu, Y., Burgon, T.B., Estes, J.D., Thacker, T.C., Crandall, K.A., McArthur, J.C., Burton, G.F., 2008. Characterization of the follicular dendritic cell reservoir of human immunodeficiency virus type 1. J. Virol. 82 (11), 5548–5561.
Kestler, H., Kodama, T., Ringler, D., Marthas, M., Pedersen, N., Lackner, A., Regier, D., Sehgal, P., Daniel, M., King, N., et al., 1990. Induction of AIDS in rhesus monkeys by molecularly cloned simian immunodeficiency virus. Science 248 (4959), 1109–1112.
Koyanagi, Y., Harada, S., Yamamoto, N., 1986. Establishment of a high production system for AIDS retroviruses with a human T-leukemic cell line Molt-4. Cancer Lett. 30 (3), 299–310.
Markowitz, M., Louie, M., Hurley, A., Sun, E., Di Mascio, M., Perelson, A.S., Ho, D.D., 2003. A novel antiviral intervention results in more accurate assessment of human immunodeficiency virus type 1 replication dynamics and T-cell decay in vivo. J. Virol. 77 (8), 5037–5038.
Martinez, M.A., Cabana, M., Ibanez, A., Clotet, B., Arno, A., Ruiz, L., 1999. Human immunodeficiency virus type 1 genetic evolution in patients with prolonged suppression of plasma viremia. Virology 256 (2), 180–187.
Meng, G., Sellers, M.T., Mosteller-Barnum, M., Rogers, T.S., Shaw, G.M., Smith, P.D., 2000. Lamina propria lymphocytes, not macrophages, express CCR5 and CXCR4 and are the likely target cell for human immunodeficiency virus type 1 in the intestinal mucosa. J. Infect. Dis. 182 (3), 785–791.
Miyake, A., Ibuki, K., Enose, Y., Suzuki, H., Horiuchi, R., Motohara, M., Saito, N., Nakasone, T., Honda, M., Watanabe, T., Miura, T., Hayami, M., 2006. Rapid dissemination of a pathogenic simian/human immunodeficiency virus to systemic organs and active replication in lymphoid tissues following intrarectal infection. J. Gen. Virol. 87 (Pt 5), 1311–1320.
Murray, J.M., Emery, S., Kelleher, A.D., Law, M., Chen, J., Hazuda, D.J., Nguyen, B.Y., Teppler, H., Cooper, D.A., 2007. Antiretroviral therapy with the integrase inhibitor raltegravir alters decay kinetics of HIV, significantly reducing the second phase. AIDS 21 (17), 2315–2321.
North, T.W., Higgins, J., Deere, J.D., Hayes, T.L., Villalobos, A., Adamson, L., Shacklett, B. L., Schinazi, R.F., Luciw, P.A., 2009. Viral sanctuaries during highly active antiretroviral therapy in a nonhuman primate model for AIDS. J. Virol. 84 (6), 2913–2922.
Palmer, S., Maldarelli, F., Wiegand, A., Bernstein, B., Hanna, G.J., Brun, S.C., Kempf, D.J., Mellors, J.W., Coffin, J.M., King, M.S., 2008. Low-level viremia persists for at least 7 years in patients on suppressive antiretroviral therapy. Proc. Natl. Acad. Sci. U. S. A. 105 (10), 3879–3884.
Pantaleo, G., Graziosi, C., Demarest, J.F., Butini, L., Montroni, M., Fox, C.H., Orenstein, J. M., Kotler, D.P., Fauci, A.S., 1993. HIV infection is active and progressive in lymphoid tissue during the clinically latent stage of disease. Nature 362 (6418), 355–358.
Pauwels, R., Balzarini, J., Baba, M., Snoeck, R., Schols, D., Herdewijn, P., Desmyter, J., De Clercq, E., 1988. Rapid and automated tetrazolium-based colorimetric assay for the detection of anti-HIV compounds. J. Virol. Methods 20 (4), 309–321.
Perelson, A.S., Essunger, P., Cao, Y., Vesanen, M., Hurley, A., Saksela, K., Markowitz, M., Ho, D.D., 1997. Decay characteristics of HIV-1-infected compartments during combination therapy. Nature 387 (6629), 188–191.
Perelson, A.S., Nelson, P.W., 1999. Mathematical analysis of HIV-1 dynamics in vivo. Siam Rev. 41 (1), 3–44.
Popovic, M., Sarngadharan, M.G., Read, E., Gallo, R.C., 1984. Detection, isolation, and continuous production of cytopathic retroviruses (HTLV-III) from patients with AIDS and pre-AIDS. Science 224 (4648), 497–500.
Reagan-Shaw, S., Nihal, M., Ahmad, N., 2008. Dose translation from animal to human studies revisited. FASEB J. 22 (3), 659–661.
Reed, L., Muench, H., 1938. A simple method of estimating fifty percent endpoints. Am. J. Hyg. 27, 493–497.
Richman, D.D., 2001. HIV chemotherapy. Nature 410 (6831), 995–1001.
Sato, A., Kodama, M., Abe, K., Miki, S., Nishimura, M., Suyama, A., Ogata, M., Toyoda, T., Sugimoto, H., Yoshie, O., et al., 1995. A simple and rapid method for preliminary evaluation of in vivo efficacy of anti-HIV compounds in mice. Antiviral Res. 27 (1–2), 151–163.
Sharkey, M., Babic, D.Z., Greenough, T., Gulick, R., Kuritzkes, D.R., Stevenson, M., 2011. Episomal viral cDNAs identify a reservoir that fuels viral rebound after treatment interruption and that contributes to treatment failure. PLoS Pathog. 7 (2), e1001303.
Sharkey, M., Triques, K., Kuritzkes, D.R., Stevenson, M., 2005. In vivo evidence for instability of episomal human immunodeficiency virus type 1 cDNA. J. Virol. 79 (8), 5203–5210.
Sharkey, M.E., Teo, I., Greenough, T., Sharova, N., Luzuriaga, K., Sullivan, J.L., Bucy, R.P., Kostrikis, L.G., Haase, A., Veryard, C., Davaro, R.E., Cheeseman, S.H., Daly, J.S., Bova, C., Ellison III, R.T., Mady, B., Lai, K.K., Moyle, G., Nelson, M., Gazzard, B., Shaunak, S., Stevenson, M., 2000. Persistence of episomal HIV-1 infection intermediates in patients on highly active anti-retroviral therapy. Nat. Med. 6 (1), 76–81.
Shibata, R., Kawamura, M., Sakai, H., Hayami, M., Ishimoto, A., Adachi, A., 1991. Generation of a chimeric human and simian immunodeficiency virus infectious to monkey peripheral blood mononuclear cells. J. Virol. 65 (7), 3514–3520.
Siliciano, J.D., Kajdas, J., Finzi, D., Quinn, T.C., Chadwick, K., Margolick, J.B., Kovacs, C., Gange, S.J., Siliciano, R.F., 2003. Long-term follow-up studies confirm the stability of the latent reservoir for HIV-1 in resting CD4+ T cells. Nat. Med. 9 (6), 727–728.

Spiegel, H., Herbst, H., Niedobitek, G., Foss, H.D., Stein, H., 1992. Follicular dendritic cells are a major reservoir for human immunodeficiency virus type 1 in lymphoid tissues facilitating infection of CD4+ T-helper cells. Am. J. Pathol. 140 (1), 15–22.

Thacker, T.C., Zhou, X., Estes, J.D., Jiang, Y., Keele, B.F., Elton, T.S., Burton, G.F., 2009. Follicular dendritic cells and human immunodeficiency virus type 1 transcription in CD4+ T cells. J. Virol. 83 (1), 150–158.

Van Rompay, K.K., Brignolo, L.L., Meyer, D.J., Jerome, C., Tarara, R., Spinner, A., Hamilton, M., Hirst, L.L., Bennett, D.R., Canfield, D.R., Dearman, T.G., Von Morgenland, W., Allen, P.C., Valverde, C., Castillo, A.B., Martin, R.B., Samii, V.F., Bendele, R., Desjardins, J., Marthas, M.L., Pedersen, N.C., Bischofberger, N., 2004. Biological effects of short-term or prolonged administration of 9-[2-(phosphonomethoxy)propyl]adenine (tenofovir) to newborn and infant rhesus macaques. Antimicrob. Agents Chemother. 48 (5), 1469–1487.

Veazey, R.S., DeMaria, M., Chalifoux, L.V., Shvetz, D.E., Pauley, D.R., Knight, H.L., Rosenzweig, M., Johnson, R.P., Desrosiers, R.C., Lackner, A.A., 1998. Gastrointestinal tract as a major site of CD4 + T cell depletion and viral replication in SIV infection. Science 280 (5362), 427–431.

Veazey, R.S., Mansfield, K.G., Tham, I.C., Carville, A.C., Shvetz, D.E., Forand, A.E., Lackner, A.A., 2000. Dynamics of CCR5 expression by CD4(+) T cells in lymphoid tissues during simian immunodeficiency virus infection. J. Virol. 74 (23), 11001–11007.

Witvrouw, M., Pannecouque, C., Switzer, W.M., Folks, T.M., De Clercq, E., Heneine, W., 2004. Susceptibility of HIV-2, SIV and SHIV to various anti-HIV-1 compounds: implications for treatment and postexposure prophylaxis. Antivir. Ther. 9 (1), 57–65.

Wong, J.K., Hezareh, M., Gunthard, H.F., Havlir, D.V., Ignacio, C.C., Spina, C.A., Richman, D.D., 1997. Recovery of replication-competent HIV despite prolonged suppression of plasma viremia. Science 278 (5341), 1291–1295.

Web reference

Department of Health and Human Services (DHHS), 2011. Guidelines for the use of antiretroviral agents in HIV-1-infected adults and adolescents. http://aidsinfo.nih.gov/contentfiles/AdultandAdolescentGL.pdf2011.

Iwami et al. Retrovirology 2012, 9:18
http://www.retrovirology.com/content/9/1/18

RETROVIROLOGY

RESEARCH Open Access

Quantification system for the viral dynamics of a highly pathogenic simian/human immunodeficiency virus based on an *in vitro* experiment and a mathematical model

Shingo Iwami[1,2,3,6*], Benjamin P Holder[4], Catherine AA Beauchemin[4], Satoru Morita[5], Tetsuko Tada[3], Kei Sato[3], Tatsuhiko Igarashi[3] and Tomoyuki Miura[3*]

Abstract

Background: Developing a quantitative understanding of viral kinetics is useful for determining the pathogenesis and transmissibility of the virus, predicting the course of disease, and evaluating the effects of antiviral therapy. The availability of data in clinical, animal, and cell culture studies, however, has been quite limited. Many studies of virus infection kinetics have been based solely on measures of total or infectious virus count. Here, we introduce a new mathematical model which tracks both infectious and total viral load, as well as the fraction of infected and uninfected cells within a cell culture, and apply it to analyze time-course data of an SHIV infection *in vitro*.

Results: We infected HSC-F cells with SHIV-KS661 and measured the concentration of Nef-negative (target) and Nef-positive (infected) HSC-F cells, the total viral load, and the infectious viral load daily for nine days. The experiments were repeated at four different MOIs, and the model was fitted to the full dataset simultaneously. Our analysis allowed us to extract an infected cell half-life of 14.1 h, a half-life of SHIV-KS661 infectiousness of 17.9 h, a virus burst size of 22.1 thousand RNA copies or 0.19 $TCID_{50}$, and a basic reproductive number of 62.8. Furthermore, we calculated that SHIV-KS661 virus-infected cells produce at least 1 infectious virion for every 350 virions produced.

Conclusions: Our method, combining *in vitro* experiments and a mathematical model, provides detailed quantitative insights into the kinetics of the SHIV infection which could be used to significantly improve the understanding of SHIV and HIV-1 pathogenesis. The method could also be applied to other viral infections and used to improve the *in vitro* determination of the effect and efficacy of antiviral compounds.

Keywords: Viral infectiousness, Quantification of viral dynamics, *In vitro* experiment, Mathematical model, Simian/Human immunodeficiency virus

Background

Historically, the study of the highly pathogenic simian/human immunodeficiency virus (SHIV) has provided important information for the understanding of human immunodeficiency virus type-1 (HIV-1) pathogenesis. For example, it was clarified in an SHIV animal study that co-receptor usage determined by the HIV-1 *env* gene affects the virus' cell tropism (preference for specific target cell populations), and thus its pathogenesis, *in vivo* [1-3]. Furthermore, infections with highly pathogenic SHIV strains in animal models have exhibited stable clinical manifestations in most infected animals, similar to an aspect of infection course in human HIV infections [4,5]. One of the highly pathogenic SHIV strains, SHIV-KS661, which has the *env* gene of HIV-1 89.6 and predominantly uses CXCR4 as the secondary receptor for its infection [2], causes an infection that

* Correspondence: siwami@ms.u-tokyo.ac.jp; tmiura@virus.kyoto-u.ac.jp
[1]Precursory Research for Embryonic Science and Technology (PRESTO), Japan Science and Technology Agency (JST), Kawaguchi, Saitama 332-0012, Japan
[3]Institute for Virus Research, Kyoto University, Kyoto, Kyoto 606-8507, Japan
Full list of author information is available at the end of the article

systemically depletes the $CD4^+$ T cells of rhesus macaques within 4 weeks after infection [6,7]. In observations by our group in recent years, the intravenous infection of rhesus macaques with SHIV-KS661 has consistently resulted in high viremia and $CD4^+$ T cell depletion, followed by malignant morbidity as a result of severe chronic diarrhea and wasting after 6 to 18 months [8]. Despite this well-developed *in vivo* model, the detailed kinetics of SHIV-KS661 remain unclear. Quantifying and understanding viral kinetics will provide us with novel insights about the pathogenesis of SHIV (and HIV-1), for example, by enabling the quantitative comparison of the replicative capacity of different strains.

In recent years, virological data from clinical patient studies, animal experiments, and cell culture studies have frequently been analyzed using mathematical models. Mathematical analysis of clinical data is an increasingly popular tool for the evaluation of drugs, the elaboration of diagnostic criteria, and the generation of recommendations for effective therapies [9-17]. Analyses of animal and cell culture studies have revealed fundamental aspects of viral infections including the specification of the half-life of infected cells and virus, the virus burst size, and the relative contribution of the immune response [18-29]. Important results have also been obtained in the analysis of purely *in vitro* experiments. For example, in Beauchemin *et. al.* [19], simple mathematical models were employed to analyze the effect of amantadine treatment on the course of experimental infections of Madin Darby canine kidney (MDCK) cells with influenza A/Albany/1/98 (H3N2) in a hollow-fiber (HF) reactor. Fits of the models to the experimental data determined that the 50% inhibitory concentration (IC_{50}) of amantadine for that particular strain was 0.3-0.4 μM and found amantadine to be 56-74% effective at blocking the infection of target cells. Thus, analyses of experimental data using mathematical models have provided, and continue to provide, quantitative information about the kinetics of viral infections - particularly for HIV-1, the hepatitis C virus (HCV), and the influenza virus - by estimating infection parameters buried within experimental data.

Despite these successes, the available virological data, even for *in vitro* experiments, have often been limited in that many modeling analyses have been based only on total viral load data (e.g., RNA or DNA copies, hemagglutination assay (HA)) [9-13,15-17,20,22,23,26,27] or infectious viral load data (e.g., 50% tissue culture infection dose ($TCID_{50}$) or plaque forming units (PFU)) [18,19,25]. Thus, while the applied mathematical models typically depend on the interaction of many components of the infection - including the populations of susceptible and infected cells - they are often only confronted by a single biological quantity: the time-course of the viral load. More rarely, diverse data sets including both virus and cell measurements have been considered [14,29-37]. Notable examples of the latter case include the analysis of an influenza infection in a microcarrier culture by Schulz-Horsel *et al.* [29], who measured and modeled the infectious and total viral load, along with the fraction of infected cells; and the *in vivo* studies of HIV-1 dynamics following antiviral therapy by Perelson and co-workers (e.g., [14,31]), who have considered measurements of viral load as well as susceptible and infected cells.

Here, we combined a relatively simple mathematical model of SHIV infection in HSC-F cells with an *in vitro* experimental system which allows for the measurement of both total and infectious viral load and the concentration of target and infected cells. We infected HSC-F - a $CD4^+$ T cell line established from cynomolgus monkey - *in vitro* with SHIV-KS661 at four different multiplicities of infection (MOI) and measured the concentration of Nef-negative (susceptible/target) and Nef-positive (infected/virus producing) HSC-F cells [cells/ml], and the total [RNA copies/ml] and infectious [$TCID_{50}$/ml] viral load daily over nine days. With this abundant and diverse data, we were able to fully parameterize the dynamic model and determine robust estimates for viral kinetics parameters, thus quantifying the infection cycle. Our *in vitro* quantification system for SHIV-KS661 should be a valuable complement to the well-developed *in vivo* model and can be used to significantly improve the understanding of SHIV and HIV-1 pathogenesis.

Results

Mathematical model

To describe the *in vitro* kinetics of the SHIV-KS661 viral infection in our experimental system (Table 1), we expanded a basic mathematical model widely used for analyzing viral kinetics [13,17-19,27,38,39]. The following equations are our extended model:

$$\frac{dx}{dt} = -\beta x v_I - dx \tag{1}$$

$$\frac{dy}{dt} = \beta x v_I - ay \tag{2}$$

$$\frac{dv_I}{dt} = pky - r_I v_I - r_{RNA} v_I \tag{3}$$

$$\frac{dv_{NI}}{dt} = (1-p)ky + r_I v_I - r_{RNA} v_{NI} \tag{4}$$

where x and y are the number of target (susceptible) and infected (virus-producing) cells per ml of medium,

Table 1 Experimental data for the *in vitro* experiment

MOI	Measurement day								
	0	1	2	3	4	5	6	7	8
Concentration of Nef-negative HSC-F cells (cells/ml)									
2×10^{-3}	5470829	6044623	2690861	1012828	223584	42130	58470	10386	10270
2×10^{-4}	2333804	4953074	2985268	2201172	811240	621750	60255	19998	4857
2×10^{-5}	2574201	3563431	3434160	2345412	1269216	1345728	264794	71792	127996
2×10^{-6}	3357117	2583058	4557411	35074989	1334060	1896048	1022157	307908	153360
Concentration of Nef-positive HSC-F cells (cells/ml)									
2×10^{-3}	d.l.*	d.l.	439139	1167172	736416	177870	41530	19614	9730
2×10^{-4}	d.l.	d.l.	84732	158828	548760	878250	89745	40002	5143
2×10^{-5}	d.l.	d.l.	d.l.	64588	170784	574272	165206	88208	92004
2×10^{-6}	d.l.	d.l.	d.l.	d.l.	65940	383952	347843	232092	86640
Total viral load of SHIV-KS661 (RNA copies/ml)									
2×10^{-3}	9180000	331000000	2840000000	4050000000	3140000000	1120000000	154000000	20200000	5650000
2×10^{-4}	1030000	26200000	256000000	1670000000	2110000000	1740000000	609000000	134000000	19400000
2×10^{-5}	126744	4370000	51200000	489000000	1280000000	1940000000	1230000000	570000000	130000000
2×10^{-6}	10170	800536	4600000	54200000	322000000	1300000000	1210000000	603000000	275000000
Infectious viral load of SHIV-KS661 ($TCID_{50}$/ml)									
2×10^{-3}	40	4064	40960	81920	163840	20480	2560	160	d.l.
2×10^{-4}	d.l.	101	403	5120	16255	40960	1280	101	40
2×10^{-5}	d.l.	64	640	4064	20480	25803	5120	1280	640
2×10^{-6}	40	40	80	640	5120	1280	1280	640	1280

"d.l." designates samples in which the concentration was below the detection limit.

v_I and v_{NI} are the number of RNA copies of infectious and non-infectious virus per ml of medium, respectively. Parameters d, a, r_{RNA}, and β represent the death rate of target cells, the death rate of infected cells, the degradation rate of viral RNA, and the rate constant for infection of target cells by virus, respectively. We assume that each infected cell releases k virus particles per day (i.e., k is the viral production rate of an infected cell), of which a fraction p are infectious and 1-p are non-infectious. Infectious virions lose infectivity at rate r_I, becoming non-infectious. Implicit in Eqs.(1)-(4) is the assumption that once a cell is infected by infectious virus it immediately begins producing progeny virus. We also tested a variant of the model which incorporates an "eclipse" phase of infection to represent the cell's period of latency prior to virus production. We found, however, that including this phase did not significantly improve the fit of the model to the data and led to very similar extracted parameter values (see Additional files 1, 2, 3). Therefore, in all further analyses, this phase was omitted in favor of the simpler model formulation. A schematic of our mathematical model is shown in Figure 1.

To fit the observed viral load data - consisting of RNA copies/ml and $TCID_{50}$/ml - and to account for the partial removal of cells and virus due to sampling, we transformed Eqs.(1)-(4) into the following scaled model:

$$\frac{dx}{dt} = -\beta_{50} x v_{50} - dx - \delta x \tag{5}$$

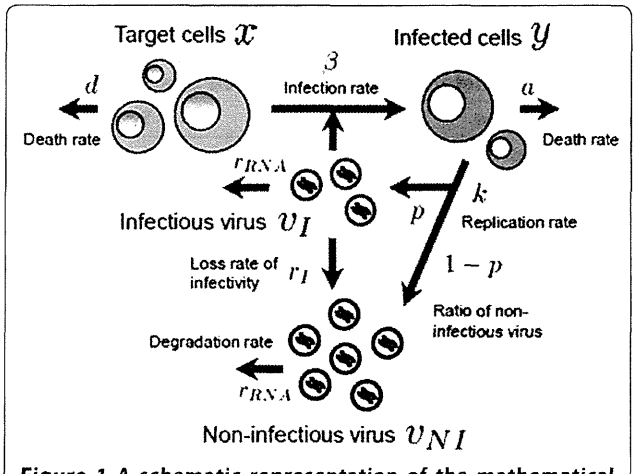

Figure 1 A schematic representation of the mathematical model. The variables x and y are the number of target and infected cells; v_I and v_{NI} are the number of RNA copies of infectious and non-infectious virus, respectively. Parameters d, a, r_{RNA}, and β represent the death rate of target cells, the death rate of infected cells, the degradation rate of viral RNA, and the rate constant for infection of cells by infectious virus, respectively. It is assumed that infected cells release virus particles at a rate k, that a fraction p of these particles are infectious (1-p are non-infectious) but lose infectivity at a rate r_I, becoming non-infectious.

$$\frac{dy}{dt} = \beta_{50} x v_{50} - a y - \delta y \quad (6)$$

$$\frac{dv_{RNA}}{dt} = k y - r_{RNA} v_{RNA} - r_c v_{RNA} \quad (7)$$

$$\frac{dv_{50}}{dt} = k_{50} y - r_I v_{50} - r_{RNA} v_{50} - r_c v_{50} \quad (8)$$

where $v_{RNA} = v_I + v_{NI}$ is the total concentration of viral RNA copies, $v_{50} = \alpha v_I$ is the infectious viral load expressed in $TCID_{50}$/ml, and α is the conversion factor from infectious viral RNA copies to $TCID_{50}$. Since the measure of 1 $TCID_{50}$ corresponds to an average of 0.68 infection events (by Poisson statistics), we have $0 < \alpha \leqq 1.47$ $TCID_{50}$ per RNA copies of infectious virus. Parameters $\beta_{50} = \beta/\alpha$ and $k_{50} = \alpha pk$ are the converted infection rate constant and production rate of infectious virus, respectively. At each sampling time, the concentration of Nef-negative and Nef-positive HSC-F cells must be reduced in our model by 5.5% and the viral loads (RNA copies and $TCID_{50}$) by 99.93% to account for the experimental harvesting of cells and virus. These losses were modeled in Eqs.(5)-(8) by approximating the sampling of cells and virus as a continuous exponential decay, yielding a rate of $\delta = 0.057$ per day for cell harvest and $r_c = 7.31$ per day for virus harvest. We found that a model which implements the sampling explicitly, as a punctual reduction at each sampling time, similar to the model in [19], did not significantly improve the quality of the fit (data not shown).

Of the seven free model parameters remaining, three of them (d, r_I, r_{RNA}) were determined by direct measurements in separate experiments described below. The remaining four parameters (β_{50}, a, k, k_{50}) along with 16 initial ($t = 0$) values for the variables (four at each of the four MOI values) were determined by fitting the model to the data as described in **Methods** (Tables 2 and 3).

In vitro half-lives of the SHIV-KS661 virus and HSC-F cells

The rates at which SHIV-KS661 virions lose infectivity, r_I, and the rate at which their viral RNA degrades, r_{RNA}, were each estimated directly in separate experiments (Figure 2). Linear regressions were performed to fit $\log v_{RNA}(t) = \log v_{RNA}(0) - r_{RNA} t$ and $\log v_{50}(t) = \log v_{50}(0) - r_I t$ to those data, yielding values of $r_{RNA} = 0.039$ per day (95% confidence interval (95%CI): *0.013-0.065* per day) and $r_I = 0.93$ per day (95%CI: *0.44-1.4* per day). These correspond to an infectious virion half-life of *17.9* h and an RNA viability half-life of *17.7* d. The death rate of target cells, d, was also estimated directly, in a mock infection experiment where Nef-negative (target) HSC-F cells were exposed to the culture conditions of the experiment without virus (data not shown). A linear regression was performed to fit $\log x(t) = \log x(0) - (d+\delta)t$ to the time course data, yielding $d = 0.21$ per day (95% CI: *0.18-0.27*), corresponding to an average target cell lifespan of *4.76* d (half-life of *3.30* d).

Time-course *in vitro* data

Time-course *in vitro* experimental data were collected over nine days, consisting of the concentrations of Nef-

Table 2 Parameters values and derived quantities for the *in vitro* experiment

Parameter Name	Symbol	Unit	Value	95%CI
Calculated parameters for the continuous approximation of cell and virus harvest				
Harvest rate of target and infected cells	δ	day^{-1}	0.057	-
Harvest rate of total and infectious virus	r_c	day^{-1}	7.31	-
Fitted parameters from separate experiments				
Decay rate of uninfected cells	d	day^{-1}	0.21	0.17-0.26
Rate of virion infectivity loss	r_I	day^{-1}	0.93	0.44-1.4
Degradation rate of virion RNA	r_{RNA}	day^{-1}	0.039	0.013-0.065
Parameters obtained from simultaneous fit to full *in vitro* dataset				
Rate constant for infections	β_{50}	$(TCID_{50}/ml \cdot day)^{-1}$	4.95×10^{-5}	$(2.35\text{-}9.59) \times 10^{-5}$
Decay rate of infected cells	a	day^{-1}	1.18	0.85-1.26
Production rate of total virus	k	RNA copies·day^{-1}	2.61×10^{4}	$(1.55\text{-}3.70) \times 10^{4}$
Production rate of infectious virus	k_{50}	$TCID_{50} \cdot day^{-1}$	0.22	0.12-0.40
Quantities derived from fitted values				
Viral burst size (total)	k/a	RNA copies	2.21×10^{4}	$(1.74\text{-}2.96) \times 10^{4}$
Viral burst size (infectious)	k_{50}/a	$TCID_{50}$	0.19	0.11-0.33
Basic reproductive number (without removal)	R_0	-	62.8	51.1-76.8
Basic reproductive number (with removal)	R_0^*	-	7.01	5.70-8.45
Minimum fraction of infectious virus	k_{50}/k	$TCID_{50}$/RNA copies	8.63×10^{-6}	$(4.53\text{-}16.9) \times 10^{-6}$